International Journal of Nanomedicine

Dovepress
open access to scientific and medical research

Open Access Full Text Article

ORIGINAL RESEARCH

A Sustained-Release Nanosystem with MRSA Biofilm-Dispersing and -Eradicating Abilities Accelerates Diabetic Ulcer Healing

Shan He[1,*], Huangding Wen[1,*], Nannan Yao[2], Lu Wang[3], Junqun Huang[4], Zhiqing Li[1]

[1]Department of Burns, Nanfang Hospital, Southern Medical University, Guangzhou, 510515, People's Republic of China; [2]Department of Neurology, Cangzhou Central Hospital, Cangzhou, 061000, People's Republic of China; [3]Department of Neurology, Hebei General Hospital, Shijiazhuang, 050000, People's Republic of China; [4]Department of Anaesthesia, The Seventh Affiliated Hospital, Southern Medical University, Foshan, 528000, People's Republic of China

*These authors contributed equally to this work

Correspondence: Zhiqing Li, Department of Burns, Nanfang Hospital, Southern Medical University, Guangzhou, 510515, People's Republic of China, Email lizq@smu.edu.cn

International Journal of Nanomedicine downloaded from https://www.dovepress.com/
For personal use only.

Introduction: Drug-resistant bacterial infections and biofilm formation play important roles in the pathogenesis of diabetic refractory wounds. Tea tree oil (TTO) exhibits antimicrobial, antimycotic, and antiviral activities, especially against common clinically resistant strains, such as methicillin-resistant Staphylococcus aureus (MRSA), making it a potential natural antimicrobial for the treatment of acute and chronic wounds. However, TTO is insoluble in water, volatile, light-sensitive, and cytotoxic. While previous macroscopic studies have focused on sterilization with TTO, none have sought to alter its structure or combine it with other materials to achieve sustained release.

Methods: Electrospun TTO nanoliposomes (TTO-NLs), arranged linearly via high-pressure homogenization, could stabilize the structure and performance of TTO to achieve slow drug release. Herein, we established a composite nano-sustained release system, TTO-NL/polyvinyl alcohol/chitosan (TTO-NL@PCS), using high-voltage electrospinning.

Results: Compared with the control, TTO-NL@PCS exhibits higher concentrations of the active TTO drug components, terpinen-4-ol and 1,8-cineole. Owing to its increased stability and slow release, early exposure to TTO-NL@PCS increases the abundance of reactive oxygen species in vitro, ultimately causing the biofilm to disperse and completely killing MRSA without inducing cytotoxic effects to the host. Moreover, in BKS-Lepr^{em2Cd479}/Gpt mice with a whole-layer skin infection, untargeted metabolomics analysis of wound exudates reveals upregulated PGF2α/FP receptor signaling and interleukin (IL)-1β and IL-6 expression following application of the composite system. The composite also ameliorates the chemotaxis disorder in early treatment and attenuates the wound inflammatory response during the repair stage of diabetic inflammatory wounds, and upregulates VEGF expression in the wound bed.

Conclusion: TTO-NL@PCS demonstrates the remarkable potential for accelerating diabetic and MRSA-infected wound healing.

Keywords: electrospinning, MRSA biofilm, antibacterial material, diabetic ulcer, wound healing

Introduction

Diabetic foot ulcers (DFU) have imposed severe health and economic burden globally.[1] Approximately 19–34% of diabetics are influenced by DFU and up to one-third of all diabetes care costs are estimated to be for lower-limb-related problems (about $5.9 billion annually in the United States).[2]

Previous studies have shown that in early injury, diabetic wounds are associated with neutrophil chemotaxis and decreased functional activity, making them susceptible to infection; exposure to high-glucose levels, in turn, delays the neutrophil response to injury and infection.[3] It has been speculated that such wounds might involve metabolic changes caused by neutrophils under high-glucose conditions. This microenvironment undoubtedly corresponds to a natural medium that encourages bacterial growth.

Received: 29 March 2023
Accepted: 10 July 2023
Published: 19 July 2023

© 2023 He et al. This work is published and licensed by Dove Medical Press Limited. The full terms of this license are available at https://www.dovepress.com/terms.php and incorporate the Creative Commons Attribution – Non Commercial (unported, v3.0) License (http://creativecommons.org/licenses/by-nc/3.0/). By accessing the work you hereby accept the Terms. Non-commercial uses of the work are permitted without any further permission from Dove Medical Press Limited, provided the work is properly attributed. For permission for commercial use of this work, please see paragraphs 4.2 and 5 of our Terms (https://www.dovepress.com/terms.php).

Biofilms comprise a large number of protective cells and extracellular polymers forming dense microbial communities that prevent penetration by traditional antimicrobial drugs. Biofilm formation leads to the occurrence of antibiotic resistance, whose main mechanism includes the inactivation and alteration of drug target sites, and changes in intercellular signaling within the quorum sensing system through metabolic pathways, including a reduction in intracellular drug accumulation through efflux pumps.[4] Studies have shown that methicillin-resistant *Staphylococcus aureus* (MRSA), as a typical resistant form of the human opportunistic pathogen *S. aureus*,[5,6] is present in more than 90% of chronic wounds and can cause excessive inflammation, leading to the prolonged release of inflammatory cytokines and activation of immune complexes, consequently impairing skin wound healing.[7,8] Therefore, the early inhibition of biofilm formation and complete clearance of bacteria in the deep and dormant phase of the wound are particularly important for the timely reversal of subsequent excessive inflammatory responses. Indeed, correcting abnormal neutrophil functions and effectively downregulating the inflammatory response is thought to represent a key strategy for addressing the challenges in diabetic wound treatment.

The abuse of antibiotics has caused widespread drug resistance and the production of superbacteria. Therefore, natural plant extracts with good bactericidal properties, such as tea tree oil (TTO), have gradually been increasingly considered as alternative treatment options. TTO is a volatile natural plant essential oil obtained through steam distillation of the terminal branches and leaves of *Melaleuca*, a native Australian plant, and is commonly used to treat skin infections.[9] In fact, TTO has been used over centuries for the treatment of wounds in Australian folk medicine;[10,11] subsequent findings regarding its potent antibacterial activities in inhalation treatment, aseptic surgery, dental surgery, wound disinfection, and oral irrigation have been published.[12] Indeed, TTO exhibits a broad range of antimicrobial activities against bacteria, fungi, viruses, and microorganisms that are resistant to traditional drugs.[11,13] Terpinen-4-ol[14] and 1,8-cineole[15] are its main physiologically active components, constituting approximately 30–48% of TTO, with significant killing activity against most bacteria, fungi, and viruses. The distribution ranges and chemical structures of the 15 major components of TTO are listed in Table 1.[16] More specifically, TTO inhibits P-related inflammatory reactions and regulates the release of P-initiated endothelial nitric oxide, which reduces the production of superoxide ions and pro-inflammatory factors.[17] However, TTO is insoluble in water, highly volatile, and undergoes swift oxidation when exposed to light, temperature,

Table 1 Major Components of Pure Australian Tea Tree Oil (TTO) and the Distribution Range (ISO 4730: 2017 Standard)

Component	Minimum (%)	Maximum (%)
Terpinen-4-ol	35.00	48.00
* R isomer ratio	67.00	71.00
* S isomer ratio	29.00	33.00
γ-Terpinene	14.00	28.00
α-Terpinene	6.00	12.00
1,8-Cineole	<0.01	10.00
p-Cymene	0.50	8.00
Terpinolene	1.50	5.00
α-Terpineol	2.00	5.00
α-Pinene	1.00	4.00
Sabinene	<0.01	3.50
Aromadendrene	0.20	3.00

(*Continued*)

Table 1 (Continued).

Component	Minimum (%)	Maximum (%)
Ledene	0.10	3.00
δ-Cadinene	0.20	3.00
Limonene	0.50	1.50
Globulol	<0.01	1.00
Viridiflorol	<0.01	1.00

Note: *Isomers of Terpinen-4-ol.

or air, which significantly reduces its antibacterial efficiency.[18] These properties, along with its low absorption rate, hinder its practical application in the treatment of infected wounds.[19] Therefore, a new alternative involving the transformation of TTO into a drug-controlled release system to construct hybrid materials with outstanding biofilm-dispersion ability has been suggested.

Nano-sustained-release materials are less likely to induce bacterial resistance owing to different antimicrobial mechanisms; hence, they have received increasing research attention to combat bacterial biofilm infections.[20,21] Small-volume and high-surface-area nanomaterials can efficiently invade biofilms and adhere to the deep layers of the infected tissue; as such, they often serve as carriers for slow-release antibiotics to achieve long-term antibacterial effects.[22,23] Meanwhile, liposomes comprise a lipophilic lipid bilayer and an aqueous solution core lipid-based vesicle system, which can be modified by various ligands to achieve immune evasion and targeted delivery.[24] Thus, liposomes are the most widely studied and successful drug delivery systems. Although the inclusion of TTO into nanoliposomes elicits anti-edema properties and improved skin wound-healing effect, its stability is poor.[25] We believe that the transformation of TTO into hydrophilic nanoscale liposomes is necessary for the construction of an ordered composite nanoscale slow-release system.

Recently, the electrospinning technique has been broadly applied, with encouraging results obtained in the generation of wound dressings due to its nano-sized structure.[26,27] The electrospinning process begins by charging a liquid droplet to form a cone-shaped jet (ie, Taylor cone). The charged jet is then extended along a straight line and subsequently thinned via the application of an electric field and increased electrical bending instability. Finally, the jet is solidified and collected on a grounded collector.[28] Jet bending violates axisymmetric properties and is equivalent to enhancing the stirring mode, providing the polymer fiber with high tensile properties and unique advantages, including a large surface area to volume ratio, high porosity, and small pore size.[29] However, when selecting the materials for the design of an electrospun wound dressing, absorptivity and oxygen permeability are primary factors to consider. For example,[30] electrospinning has been applied in the preparation of nanofibers composed of polyvinyl alcohol cross-linked with chitosan. Both materials present good biocompatibility, biodegradability, cellular binding capability, antimicrobial activity, and wound-healing effects.[31]

In this study, we aimed to develop a delivery system for the release of antimicrobial TTO, positioned as a composite dressing with a nanostructure. The purpose of this study was to improve the ordered structure of the material by altering the physical properties and embedded form of TTO to ensure its slow release. This is the first study, to our knowledge, to combine TTO nanoliposomes and electrospinning; we believe that this type of dressing will prove beneficial in clinical practice. However, the metabolic changes in the hierarchical microenvironment and signal transduction pathways involved in the antibacterial mechanism of TTO have not been fully defined, and further exploration of the relevant mechanisms is warranted to develop strategies to specifically disperse biofilms and reduce cytotoxicity. Accordingly, Kyoto Encyclopedia of Genes and Genomes (KEGG) and protein–protein interaction analyses of TTO were applied to elucidate the mechanism underlying the effects of TTO nanoliposomes (NL)/polyvinyl alcohol/chitosan (TTO-NL @PCS).[32] Following validation, the composite nano-sustained-release system reported herein was confirmed to aid in the healing of infected diabetic wounds.

Materials and Methods

Materials

The TTO crude oil extract (100% concentration) was provided by Chengetai Science and Technology, Ltd. (Zhuhai, China). Its concentration was determined as described in previous studies.[33,34] Chitosan (MW = 240 kDa) was purchased from Solarbio (Beijing, China). Polyvinyl alcohol (Mw of 85 kDa), type II collagenase, glacial acetic acid, MH agar plates, absolute ethanol (≥ 99.8%), cholestenone, phosphatide, and glutaraldehyde (25% in H_2O) were supplied by Sigma-Aldrich (St. Louis, MO, USA). Fetal bovine serum, phosphate-buffered saline (PBS), trypsin-ethylenediaminetetraacetic acid (trypsin-EDTA), and Dulbecco's minimum essential medium were purchased from Gibco (Waltham, MA, USA). MRSA (ATCC 43300) was obtained from the American Type Culture Collection (ATCC; Manassas, VA). Tween 80 and Span 80 were purchased from Biosharp (Beijing, China). The live/dead viability/cytotoxicity kit, live and dead bacterial staining kit, Cell Counting Kit-8 (CCK-8) cell viability reagent, and reactive oxygen species (ROS) assay kit (DCFH-DA) were purchased from Beyotime (Shanghai, China). Alexa Fluor 594-phalloidin, the anti-VEGF antibody (ab2350), the anti-myeloperoxidase (MPO) antibody (ab208670), Alexa Fluor 488/555- conjugated secondary antibodies, Alexa Fluor 594-donkey anti-rabbit IgG (H+L) (ab90812), and 4′,6-diamidino-2-phenylindole (DAPI) were purchased from Abcam (Cambridge, UK). HaCaT cell line and endothelial cells (HUVEC cell line) were purchased from the Cell Bank of the Medical Research Center of Nanfang Hospital (China).

Synthesis of Composite Nanofibers

Herein, 100 mg of TTO (10%), 320 mg of phospholipid, 30 mg of cholesterol, 100 mL of ethanol, and 200 mg of surfactant (Tween 80: Span 80 = 3:1) were mixed in a beaker, and a suspension was formed via mechanical stirring at 1000 rpm. After rotating the suspension in a 35 °C attemperator to remove the organic solvent, a thin layer of uniform film was formed on the inner wall of an eggplant-type flask. Approximately 2.26 g of lactose was dissolved in 200 mL of phosphate buffer (pH 5.0) and added to an eggplant-type flask with stirring at 100 rpm and 37 °C for 1 h. The addition of lactose prevented changes in particle size and reduced leakage from nanoliposomes.[35] Furthermore, the miscible liquids were dispersed for 10 min using an ultrasound bath. Finally, homogenization was conducted three times at 15,000 psi to obtain TTO nanoliposomes. The diameters and zeta potentials of TTO-NLs were measured using dynamic light scattering (DLS; Malvern Instruments, Malvern, UK) at 25 ± 1 °C.

Polyvinyl alcohol (8 g) and chitosan (2 g) was firstly dissolved in 1% aqueous acetic acid (70 mL). With the assistance of free amino groups, positively charged polyelectrolyte can be released from chitosan at a pH ranging from 2 to 6; thus, due to their high solubility compared to chitin solutions, chitosan solutions are highly viscous and complicated for electrospinning.[36] Furthermore, the 3-D network formed via strong hydrogen bonding prevents the movement of polymer chains during exposure to the electric field.[37] The TTO-NL solution obtained above was then mixed with PVP/CS solution mentioned above under magnetic stirring at weight ratios of 1:4 (TTO-NL/polyvinyl alcohol/chitosan). In the control groups, deionized water and TTO was added to obtain PVP/CS solution (8:2w/v%) and TTO/polyvinyl alcohol/chitosan solution (30:8:2 w/v%) in a 60 °C water bath to obtain the solution. The total volume of the solution obtained in each group was about 100 mL.

Electrospinning was carried out using a stainless-steel blunt-ended needle (inner diameter, 0.9 mm) connected to a DC power supply electrode (high-voltage power, 20 kV), syringe pump, syringe, and grounded aluminum foil. The blunt-tip metal needle was infused with various blended solutions at a feed rate of 0.6 mL/h. The distance between the needle tip and the ground collector was 15 cm (Scheme 1).

Hybrid Mechanical Characterization and Degradation Rate Assay

Morphological characterization of TTO@PCS and TTO-NL@PCS was performed using scanning electron microscopy (SEM; Sigma300, ZEISS) and atomic force microscopy (AFM; Dimension ICON, BRUKER). Sample degradation was assessed by first obtaining the original dry weights after lyophilization. Subsequently, the samples were incubated in collagenase type II solution (2 U/mL) at 37 °C in a balanced state. At preset time points, the electrospun residues were

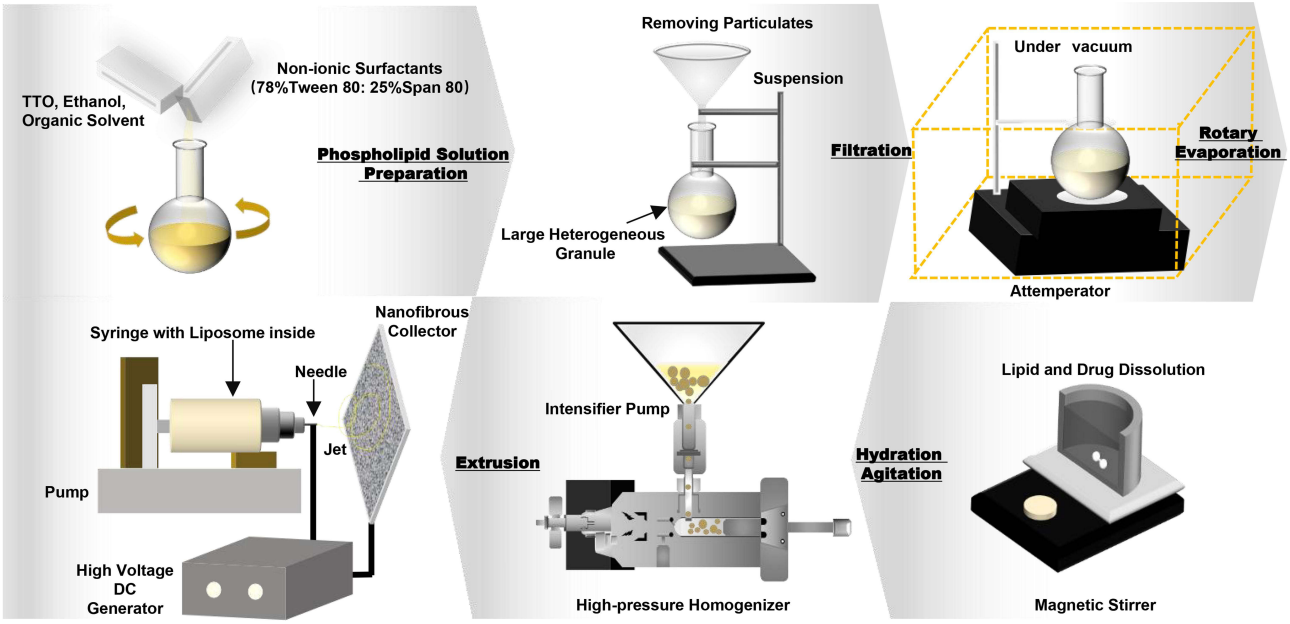

Scheme 1 Schematic representation of TTO-NLs and the electrospinning apparatus.

retrieved, lyophilized, and weighed. The masses of the hydrogel residues were compared with their initial masses to determine the degradation rate.

Release Profile of TTO

The electrospinning mats were cut into 1 cm^2 squares and placed in 5 mL of PBS (100 mM, pH 7.4, and pH 5.0). At the preset time points (6, 12, 24, 48, 72 hour), 1 mL of the release medium was removed and replenished with 1 mL of fresh buffer. The amount of drug released was determined using UV–visible spectrophotometry (NanoDrop™ One, Thermo Scientific, USA). In other words, the absorbance of the drug was obtained at 299 nm and the concentration was determined using a calibration curve. The drug release profiles were calculated from the TTO concentration at each time point.[30]

To further confirm the encapsulation efficiency, terpinen-4-ol and 1,8-cineole were analyzed as the active ingredients of TTO within composite nanosystems via gas chromatography (GC) using a flame ionization detector (FID) system,[38] equipped with an SE-30 universal type quartz capillary column (30 m × 0.2 mm × 0.25 μm) connected to a FID, according to the protocol published by Rodríguez-Maecker et al[39] The mixture was maintained at 60 °C for 3 min, followed by a 2 °C/min increase to 160°C and subsequently to 210 °C at 4 °C/min for 5 min. TTO components were identified on the basis of the retention index and mass spectrum data.[40]

Cytotoxicity Assay

For cytotoxicity assays, HaCaT and HUVEC cells were seeded in 96-well plates at a density of 5.0×10^3 cells per well for 24 h and co-cultured with nanofiber samples for an additional 24 h. Subsequently, 100 μL CCK-8 solution was added to each well and incubated for 2 h to assess cytotoxicity. Following incubation, the culture media was collected, and the absorbance was determined using a SmartReader 96 plate reader at 450 nm.

Cell viability was evaluated using a live/dead viability/cytotoxicity kit. HaCaT cells growing on the electrospinning surfaces were stained and imaged using laser scanning confocal microscopy (LSCM; LSM-980, Carl Zeiss Inc., Jena, Germany). Live (green fluorescence) and dead (red fluorescence) cells were quantified using ImageJ software. The percentage of live cells was calculated by dividing the number of live cells by the total number of cells. The cytoskeleton and nuclei were stained using Alexa Fluor 594-phalloidin and DAPI, respectively, to assess the morphological

abnormalities and diffusion area of cells on the electrospinning surface. The average number of cells was recorded from at least three independent experiments.

Antibacterial Assay

The antibacterial ability of various electrospinning samples was assessed using ATCC 43300 (MRSA). In brief, the bacteria were co-cultured with samples at an initial concentration of 1.0×10^6 (CFU) mL^{-1} in lysogeny broth (LB) medium at 37 °C, 5% CO_2. Culture LB medium was collected after 6, 12, and 24 h and centrifuged at 1000 rpm for 5 min (500 × *g*). The resultant bacteria were diluted in PBS for Live/Dead Viability staining. Green fluorescent (live) and red fluorescent (dead) bacteria were quantified under fluorescence microscopy.[41] Bactericidal activity was determined by dividing the number of dead bacteria by the total number of bacteria. Meanwhile, the antibacterial activity was macroscopically determined using a zone inhibition assay. In other words, electrospun nanofibers (size: 1×1 cm^2) were placed on agar plates with 100 μL of MRSA solution (10^8 CFU mL^{-1}) and grown at 37 °C with 5% CO_2. To compare antibacterial activity, PCS, TTO@PCS, and TTO-NL@PCS groups were created. After 1 day of incubation, the diameters and areas of the bacteriostatic rings were measured using ImageJ software, and each sample was analyzed in triplicate.

In vitro Simulated Biofilm-Dispersion Assay

In vitro MRSA Biofilm Growth on Plates

Herein, 100 μL of 5×10^8 CFU mL^{-1} MRSA was cultivated in a 96-well plate at 37 °C to generate biofilms. After removing the original medium, 200 μL of LB medium was added to each well, along with 5×5 mm^2 of the electrospun sample. The non-processed group was used as the negative control. All groups were cultured for 24 h at 37 °C. Any bacterial cells dissociated from the biofilm (planktonic) were removed by washing with saline. The biofilm was then incubated at 60 °C for 60 min and treated with a 200 μL suspension of 0.1% crystal violet for 10 min. The plates were then washed with saline to remove planktonic cells and, subsequently, treated with 200 μL ethanol for 15 min before being transferred to a new plate. The absorbance of all samples was measured at 550 nm using a microplate reader. Biofilm formation was determined based on the difference between the average OD readings obtained in the positive control (culture medium and bacteria) and the negative control (culture medium only).[42] The assay was repeated three times.

MRSA (1×10^8 CFU mL^{-1}) was cultured on a glass slide for 24 h at 37 °C to form a biofilm; next, PCS, TTO@PCS, and TTO-NL@PCS were added to the culture. After the generated biofilm was washed to remove unbound cells, a live and dead bacterial staining kit was used to stain the biofilm; results were recorded, and three-dimensional reconstruction (thickness between the beginning and end of the fluorescence on the slide) was performed through LSCM. Three random fields were examined for each sample.

In vitro MRSA Biofilm Growth on Human Tissue Samples

In accordance with the principles of the Declaration of Helsinki, ethical approval was granted by the Institute of Ethics Committee of Nanfang Hospital, Southern Medical University (approval number: NFEC-2021-265). The patients provided informed consent. Healthy human skin was collected from the thigh during whole-thickness skin sheet transplantation (in male or female patients diagnosed with diabetes without other underlying diseases), without collecting any personal identifying information.

Freshly collected full-thickness human skin was cut into 12 pieces (1.0 cm × 1.0 cm × 0.3 cm), and excess fat and connective tissues were removed. Bacterial medium containing MRSA was added to an artificial scratch area on the skin tissue surface and incubated for 48 h to allow biofilm formation. The mature biofilms were validated using SEM. Bacteria on the skin surface were obtained using cotton swabs on days 1 and 3 and colonies were cultured for 24 h prior to performing diluted plate counts to compare the differences between groups. To evaluate the dispersion ability of the electrospun biofilm, biofilms on the skin surface and electrospun samples were transferred into culture vessels (35 mm × 10 mm) with LB medium. Skin was retrieved on days 1 and 3. After treatment with alcohol-gradient dehydration and freeze-drying, SEM was used to image and measure the residual biomass.

Detection of Cellular ROS

For the DCFH-DA assay, an ROS assay kit was used. Biofilms were created, and several treatments were carried out, as described in In vitro MRSA Biofilm Growth on Plates: normal saline, PCS, TTO@PCS, and TTO@PCS. Cultures were incubated at 37 °C and allowed to react with the DCFH-DA probe at a final concentration of 10 μm in the dark for 30 min. Finally, the samples were observed via LSCM, and ROS production in distinct layers of the biofilm was tracked over time using the layer scanning tool.

Antibacterial Activity in vivo

All animal experimental protocols were approved by the Animal Research Ethics Committee of Nanfang Hospital and complied with the rules of the specific pathogen-free animal laboratory of Nanfang Medical University. All methods followed the guidelines for animal subject care and use outlined in the Guide for the Care and Use of Laboratory Animals (Institute of Laboratory Animal Resources, National Academy of Sciences, Bethesda, MD, USA).

Eight-week-old BKS-Lepr^{em2Cd479}/Gpt mice (male; 40–45 g) were obtained from GemPharmatech Laboratory Animal Co., Ltd. (Guangdong, China) and allowed to acclimatize to the environment for 1 week prior to experimentation at the Laboratory Animal Center of Nanfang Hospital of the Southern Medical University under pathogen-free conditions. Circular incisions with a 12-mm diameter were made on the backs of mice in the four groups (n = 9/group) under anesthesia (pentobarbital). Subsequently, 100 μL of MRSA suspension (10^8 CFU mL^{-1}) was applied to the circular wounds to infect all animals. After 2 days of continuous infection, a 12-mm diameter piece of each electrospun fiber was placed over the circular incision to cover the infected areas. The second sham set was used as a blank control. Simultaneously, infected wounds were photographed, and their sizes were measured using the original wound size card as a guide. The body weights of the mice were recorded each week, and their serum glucose levels (mmol/L) were measured every 4 days.

In vivo Histological Analysis

Infected wound tissues from mice on days 7, 14, and 21 were immersed in 10% EDTA for 24 h before being dried in graded alcohol and embedded in paraffin. Sections cut to a thickness of 5 μm were subjected to hematoxylin and eosin (H&E) staining. All sections were examined under an optical microscope (OLYMPUS IX71, Olympus, Japan) at 36.5 °C.

The abundance of VEGF in the neonatal tissues of diabetic mice was assessed via immunofluorescence. After antigen retrieval, the paraffin-embedded slices of skin tissues were blocked with 10% BSA and treated with anti-VEGF antibody overnight at 4 °C. The slices were then incubated at 37 °C for 1 h in the dark with Alexa Fluor 488/555-labeled secondary antibodies. Finally, the nuclei was stained with DAPI, and images were captured using LSCM.

Exploration of the Antibacterial Mechanism

Metabolomics Assay

For the metabolic profiling of injured skin, wound exudates were collected from TTO-NL@PCS-treated and blank control groups on day 3 after the establishment of MRSA infection for untargeted metabolomics analysis. Briefly, the samples stored at −80 °C were thawed on ice. A 400 μL solution (methanol: water = 7:3 v/v) containing an internal standard was added to the sample and vortexed for 3 min. The sample was sonicated in an ice bath for 10 min, vortexed for 1 min, and then placed at −20 °C for 30 min. The samples were then centrifuged at 12,000 rpm for 10 min at 4 °C. The sediment was removed, and the supernatant was centrifuged again at 12,000 rpm and 4 °C for 3 min. A 200 μL aliquot of the supernatant was transferred for LC-MS analysis. All wound exudate samples were prepared according to the instrument operation requirements. The analytical conditions were as follows: ultra-performance liquid chromatography (UPLC): column, Waters ACQUITY UPLC HSS T3 C18 (1.8 μm, 2.1 mm × 100 mm); column temperature, 40 °C; flow rate, 0.4 mL/min; injection volume, 2 μL; solvent system, water (0.1% formic acid): acetonitrile (0.1% formic acid); gradient program, 95:5 v/v at 0 min, 10:90 v/v at 11.0 min, 10:90 v/v at 12.0 min, 95:5 v/v at 12.1 min, 95:5 v/v at 14.0 min.

A 10^{-6} M $PGF_{2\alpha}$ solution (Sigma-Aldrich, US) was used for subsequent experiments, which was considered appropriate to function without damaging the local tissue (Figure S1. Sham, TTO-NL@PCS, $PGF_{2\alpha}$, and TTO-NL@PCS+$PGF_{2\alpha}$ were applied separately (n = 3). For the TTO-NL@PCS+$PGF_{2\alpha}$ group, wounds with an established MRSA biofilm (Methods are shown in Antibacterial Activity in vivo) were covered with sterile gauze soaked with a specific concentration of $PGF_{2\alpha}$ for 6 h; this gauze was removed and replaced with TTO-NL@PCS. The $PGF_{2\alpha}$ group was treated with $PGF_{2\alpha}$-soaked sterile gauze for 6 h, whereas the MRSA-infected wounds were directly covered with TTO-NL@PCS in the TTO-NL@PCS group.

Isolation of RNA and Real-Time PCR Analysis

On day 7 following TTO-NL@PCS treatment, local tissues were harvested for total RNA extraction, performed using RNAiso Plus (Takara Bio, Kyoto, Japan). cDNA was synthesized using the PrimeScript™ RT reagent kit with gDNA Eraser (Perfect Real Time; Takara, Japan). Quantitative real-time polymerase chain reaction was performed using QuantStudio (Thermo Fisher, USA) with TB Green® Premix Ex Taq™ II (Takara, Japan). Primers and genes used are listed in Table 2. The data are shown as fold-changes compared to levels in the control group.

Immunofluorescence Assay in vivo

On days 1 and 7, TTO-NL@PCS was used to remove skin tissue from the wound. Deparaffinization, alcohol-gradient dehydration, and antigen retrieval were performed on paraffin slices of skin tissues treated with the various agents. After blocking with 10% BSA, the slices were incubated with an anti-MPO antibody overnight at 4 °C and subsequently incubated at 37 °C in the dark for 45 min with Alexa Fluor 488/555-labeled secondary antibodies. Images were captured with an LSCM (FV1200, Olympus) camera following DAPI staining.

Statistical Analysis

All data from at least three independent experiments were presented as the mean ± standard deviation. GraphPad was used along with an unpaired Student's *t*-test or one-way analysis of variance (ANOVA) to assess statistical significance in the experiments. The differences between two groups were analyzed using an unpaired Student's *t*-test. Differences between three or more groups were analyzed using one-way ANOVA. A P-value < 0.05 indicated significant differences.

Results

Construction and Characterization of Nanoliposomes and Electrospinning

TTO-NLs were created to minimize the TTO dose and achieve delayed release. TTO-NLs had a clear and transparent appearance with a light blue emulsion that dissolved in water, whereas TTO was a light yellow and translucent liquid that was water-insoluble (Figure 1A). The average particle size of the freshly prepared TTO-NL was 49.61 ± 2.62 nm, with a zeta potential of 8.85 ± 1.67 mV, according to DLS analysis conducted to evaluate the stability of the prepared TTO-NLs. On day 3, the mean particle size at room temperature was 71.16 ± 0.91 nm and the zeta potential was 14 ± 1.85 mV, indicating that an unstable condition had been initiated (Figure 1B–F). To overcome this instability, TTO-NLs were electrospun. The internal structure of the electric spindle was observed using AFM (Figure 2A). When observed using SEM, the TTO-NL@PCS arrangement was ordered and homogeneous, whereas the TTO@PCS arrangement exhibited droplet-like insoluble material and an uneven shape (Figure 2B and C). TTO-NL@PCS had a Young's modulus of 24.79 ± 0.86 MPa, while TTO@PCS had a Young's modulus of 74.06 ± 2.57 MPa (Figure 2D),

Table 2 Sequences of Primers Used in Quantitative Polymerase Chain Reaction

Gene	Forward 5′–3′	Reverse 5′–3′
Fp receptor	GCACATTGATGGGCAACTAGAA	GCACCTATCATTGGCATGTAGCT
IL-6	GCTACCAAACTGGATATAAT	CCAGGTAGCTATGGTACTCC
IL-1β	AGTTGACGGACCCCAAAAG	AGCTGGATGCTCTCATCAGG
18S rRNA	GGGAGCCTGAGAAACGGC	GGGTCGGGAGTGGGTAATTT

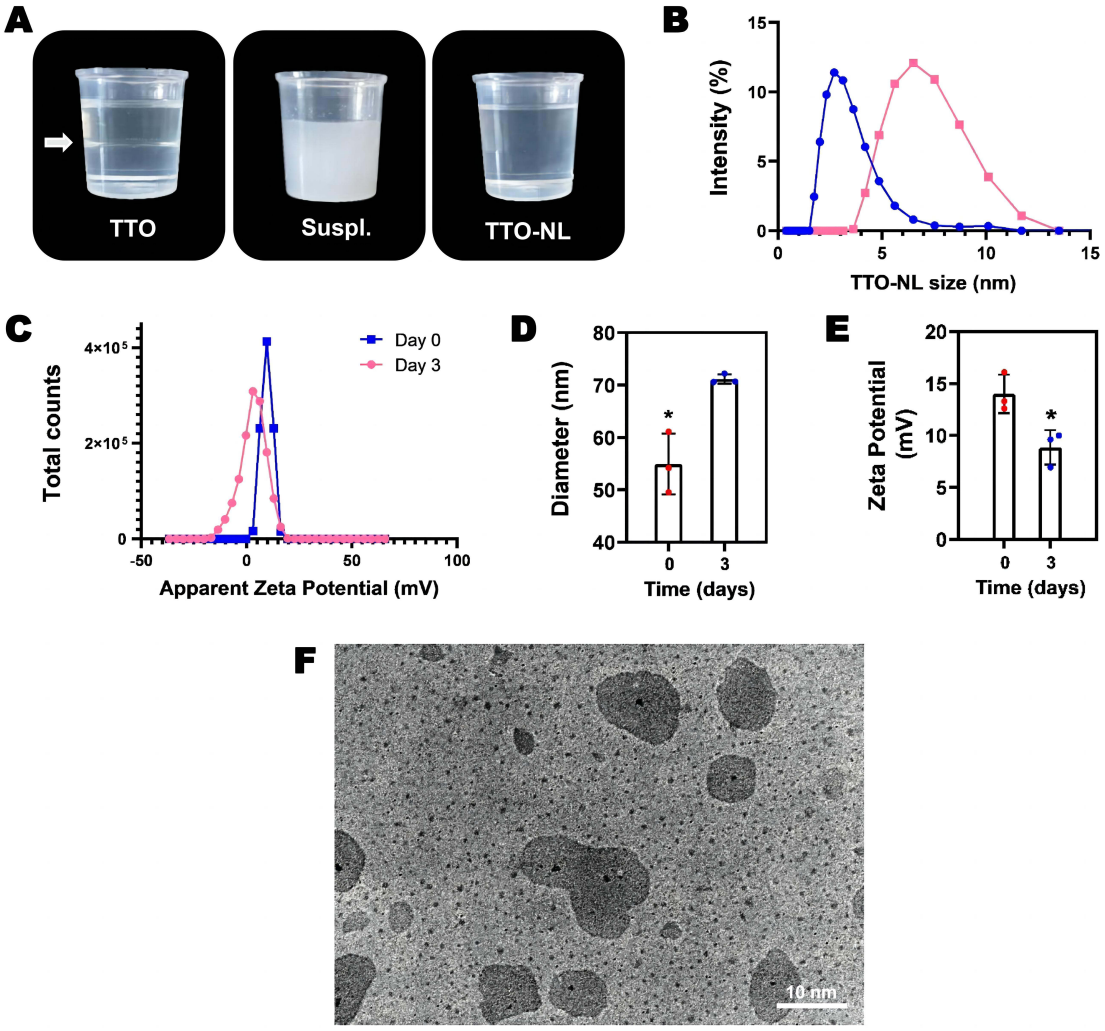

Figure 1 Physical properties of the TTO nanoliposome (TTO-NL). (**A**) TTO appearance before and after preparation and suspension status without multiple high-pressure homogenization treatments. (**B**) Diameter and (**C**) zeta potential of TTO-NLs on days 0 and 3 after preparation; (**D**) Statistical analysis of the TTO-NL diameter and (**E**) zeta potential on days 0 and 3. (**F**) The TEM image of TTO-NL. n = 3, *P < 0.05.

indicating that TTO-NL@PCS is more deformation-resistant than TTO@PCS. In terms of the electrospinning degradation rate, there was no substantial difference between TTO-NL@PCS and TTO@PCS (Figure 2E). The TTO component release rate of the extract was measured using peak UV absorption; TTO-NL@PCS released most of the drug within 72 h, whereas TTO@PCS released the drug rather quickly, with greater than 99% cumulative release within the first 24 h. Micro-environment can reflect the dynamic change during the wound healing process and pH is one of the important parameters. Acute wound, affected by active neutrophils, pH is usually between 4–6, while chronic wound is often weak alkaline between 7–8, that is more conducive to bacterial growth and reproduction and make the wound vulnerable to bacterial invasion, so does infection. Therefore, it necessary to test the drug release status in different pH, and the results showed no significant association between released-period and pH (Figure 2F), which ensure the long-term release in diabetic wound. GC was used to determine the total amount and composition of the drug released continuously in a 72 h electrospun extract. The concentrations of terpinen-4-ol and 1.8-cineole were 1.62 ± 0.29% and 0.81 ± 0.47%, respectively, indicating that the TTO concentration loaded into TTO-NL@PCS was considerably higher than that in TTO@PCS (Figure 2G–I). In our previous study,[43] the MIC of TTO for MRSA was 0.5%, while that of MBC was 2%. Thus, TTO release must be adequately controlled to maintain a safe yet effective concentration in the wound. As such, this method requires further optimization to increase the drug loading rate and achieve controlled release over an extended period of time.

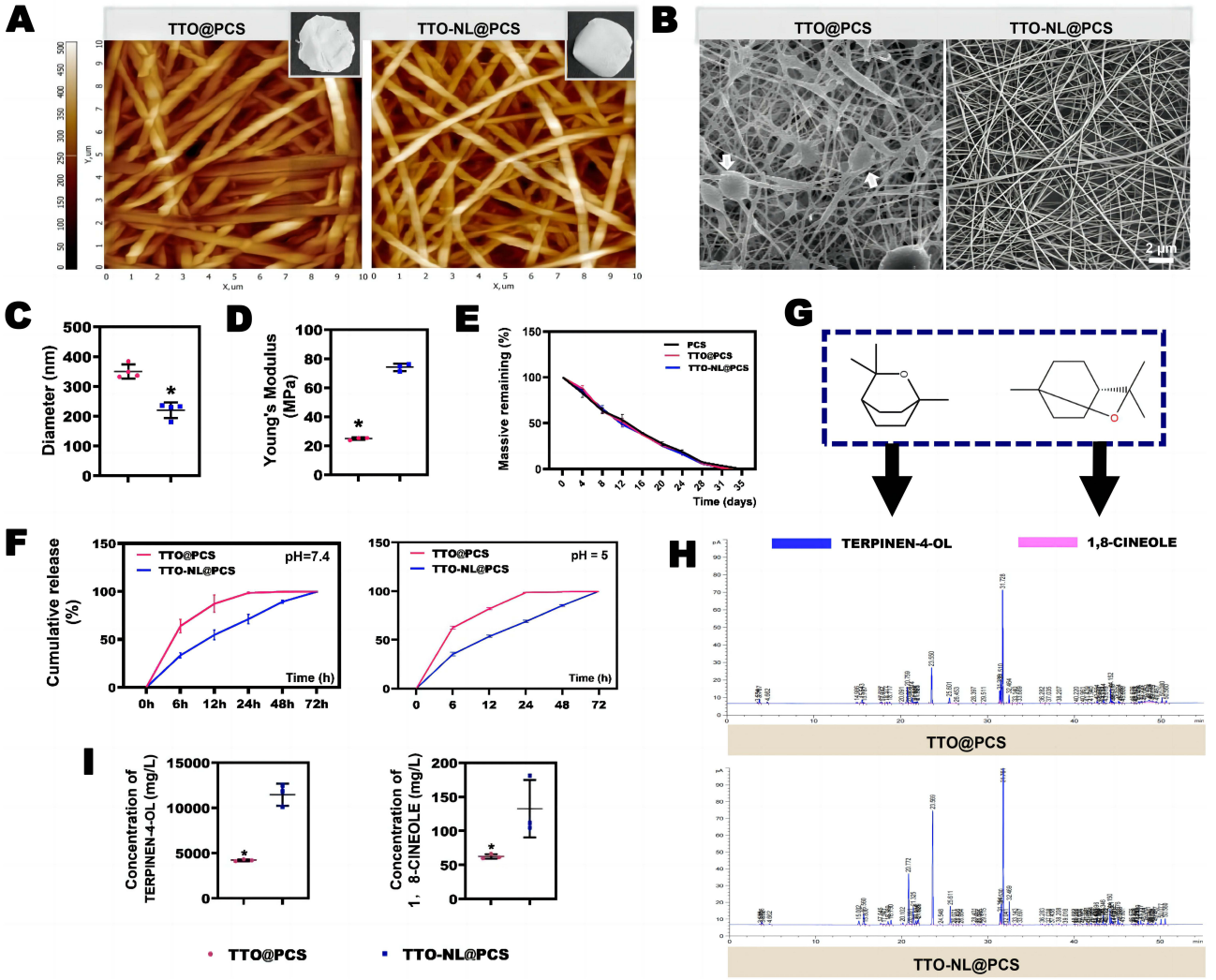

Figure 2 Fabrication and characterization of the sustained-release nanosystem. (**A**) AFM and (**B**) SEM images of TTO-NL@PCS and TTO@PCS. The electrospun appearance diagram is shown in the dashed frame. White arrows indicate the uneven diameter of the electrospun nanofibers due to insufficient binding of the oil droplets to the material. (**C**) Diameter and (**D**) Young's Modulus of TTO-NL@PCS and TTO@PCS (n = 3, *P < 0.05). (**E**) Degradation rate of electrospun nanofibers and (**F**) cumulative release profiles of TTO encapsulated in TTO-NL@PCS and TTO@PCS (in pH 7.4, and pH 5.0). (**G**) Illustration of chemical constitution. (**H**) Concentrations of the major drug components terpinen-4-ol and 1.8-cineole were quantified in a 72 h extract, and (**I**) quantitative analysis of concentrations of the drug components. n = 3, *P < 0.05.

Cell Viability and Proliferation Assays

As indicated by the live and dead staining in Figure 3A, keratinocytes (KCs) co-cultured with various electrospun samples revealed similar cell viability (Figure 3B) and cell counts (Figure 3C). The cells grown on the electrospun surface proliferated normally with no morphological abnormalities, which corresponded with the F-actin/phalloidin staining results (Figure 3D and E). Moreover, the CCK-8 results in Figure 3F show that TTO-NL@PCS, TTO@PCS, and PCS did not elicit significant cytotoxicity toward either cell type associated with wound healing.

Bactericidal Ability of Electrospun Nanofibers

Both TTO-NL@PCS and TTO@PCS showed a significant effect on bacterial growth in the inhibition zone assays. The regional diameters when TTO-NL@PCS, TTO@PCS, and PCS were added to MRSA plates were 1.23 ± 0.21, 0.644 ± 0.11, and 0 cm, respectively (Figure 4A and D). Live and dead staining was further used to verify the bactericidal effect against the MRSA strain (ATCC 43300) in a dispersed state in the LB medium, and TTO-NL@PCS showed a superior bactericidal effect. TTO-NL@PCS killed 83–87% and 99–100% of viable bacteria at 6 h and 12 h, respectively, whereas

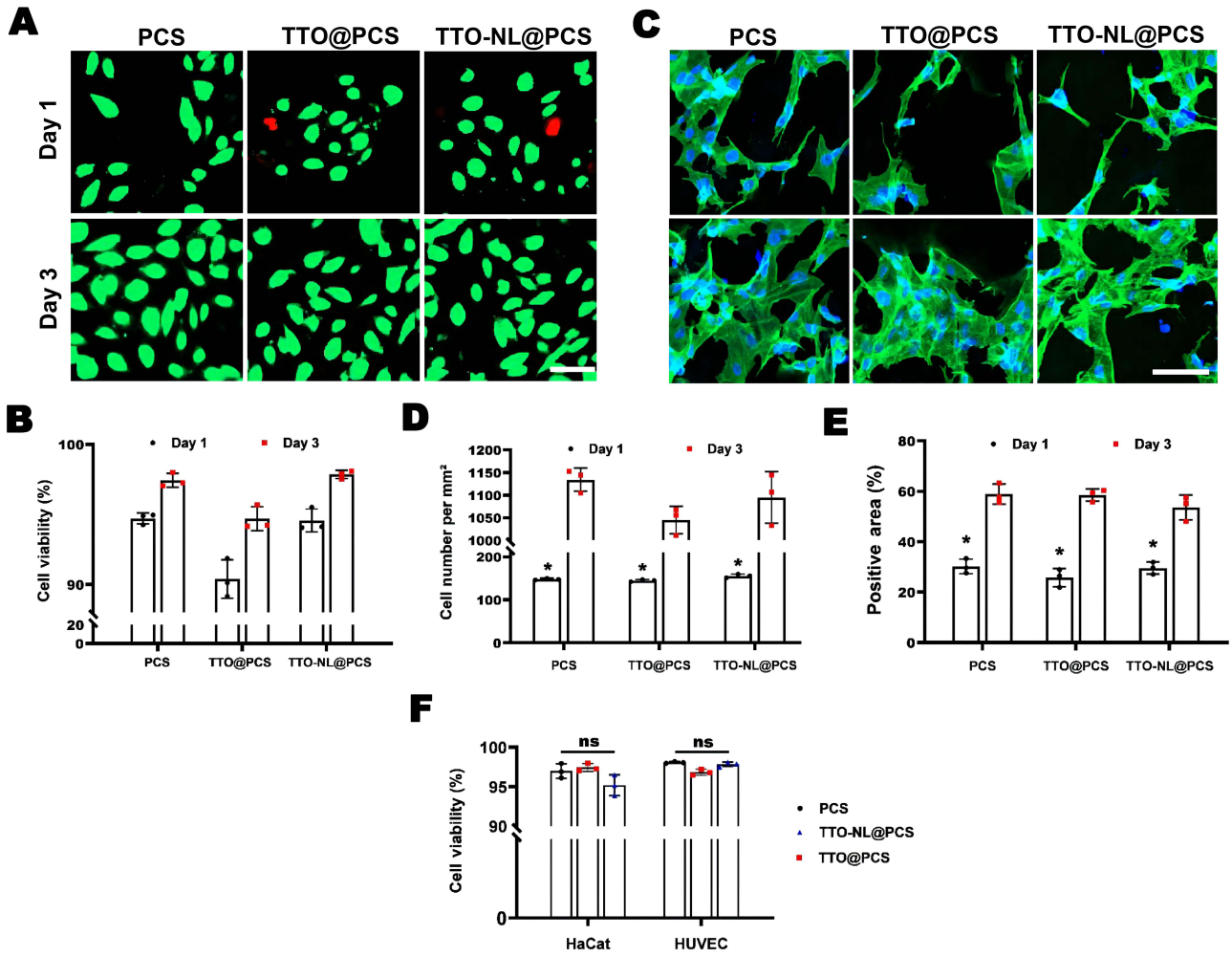

Figure 3 Cytotoxicity evaluation of the TTO-NL@PCS sustained-release nanosystem. (**A**) Live and dead staining of keratinocytes (KCs) cultivated with electrospun nanofibers on days 1 and 3; (**B** and **C**) viability and cell number analyses (green, viable cells; red, dead cells). (**D**) Phalloidin and DAPI labeling of cell proliferation on days 1 and 3, and (**E**) cell area quantification of KC proliferation on various electrospun surfaces. *P < 0.05, scale bars =100 m, n = 3 (random field of vision). (**F**) HaCaT and HUVEC cells co-cultured with equal volumes of TTO-NL@PCS, TTO@PCS, and PCS after 24 h (n = 3).

TTO@PCS killed 11–19% and 49–55% of bacteria at 6 h and 12 h, respectively; both reached 100% at 24 h (Figure 4B and E). TTO-NL@PCS demonstrated efficient and continuous biofilm-dispersion and eradicating abilities, whereas TTO@PCS did not significantly reduce the biofilm biomass by day 2. Thereafter, we determined the bactericidal efficiency of TTO-NL@PCS and TTO@PCS against adherent MRSA biofilms. There was no significant difference in the remaining biomass of the MRSA biofilm after 24 h of treatment between TTO-NL@PCS and TTO@PCS (Figure 4C and F). After 24 h of TTO-NL@PCS treatment, live bacteria were rarely detected via LSCM layer scanning, similar to that with the biofilm residue, which was compared using CV staining results (Figure 4G). At this time, more biofilm residues and living bacterial cells were observed after treatment with TTO@PCS (Figure 4H). These results suggested that TTO-NL@PCS was more bactericidal against MRSA biofilms than TTO@PCS.

Biofilm Dispersion in vitro

As per the schematic diagram shown in Figure 5A, to simulate biofilm dispersion, a mature biofilm was formed on the surface of the skin wounds from diabetic patients during in vitro culture for 2 days, and TTO-NL@PCS and TTO@PCS were then added for 24 h and 72 h. Microbial aggregation and growth on the skin surface were observed at 24 and 72 h (Figure 5B and C). TTO-NL@PCS destroyed the dense biofilm formed in the wound and killed bacteria, whereas TTO@PCS destroyed the biofilm at an early stage without complete sterilization owing to its short-term effects. Biofilm surface sampling for

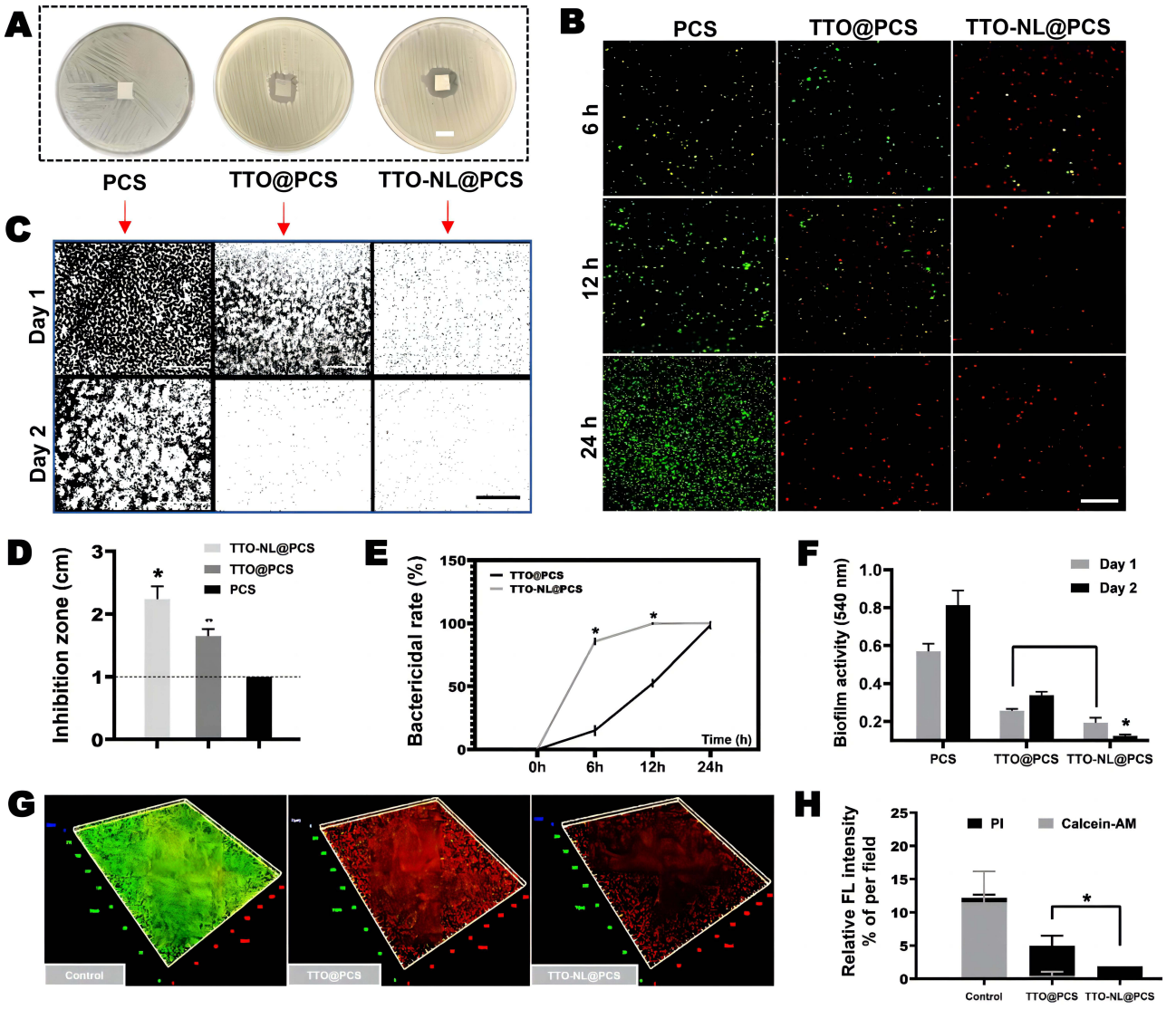

Figure 4 Inhibition zone assays and analysis of MRSA biofilm-dispersion and bactericidal abilities of electrospun nanofibers. (**A**) Inhibition zone assay results of electrospun nanofibers placed on bacteria (ATCC 43300) spread on agar plates (scale bar 1 cm), with (**D**) quantification of inhibition zone assays. (**B**) Live and dead staining results of bacteria (ATCC 43300) cultured with electrospun nanofibers at preset timepoints (scale bar 50 μm), with (**E**) quantification results of the staining results. *P < 0.05, TTO-NL @PCS vs TTO@PCS (6 h and 12 h). (**C**) Residual MRSA biofilms following treatment with electrospun nanofibers at day 1 and day 3 were stained with crystal violet and processed by ImageJ software (scale bar, 100 μm). (**F**) Relative MRSA biofilm biomass treated with different materials. MRSA biofilm biomass was determined by measuring the absorbance at 590 nm. (**G**) LSCM 3-D schematic diagram of LIVE/DEAD-stained MRSA biofilm grown on cell slides (green, viable cells; red, dead cells), and (**H**) quantification of the relative immunofluorescence intensity per field on day 1 following various electrospun nanofiber treatments. n = 3 (random field of vision), *P < 0.05.

dilution coating was used to detect bacterial colonies, which were not observed at 24 and 72 h after TTO-NL@PCS treatment (Figure 5D); hence, the few attached bacteria observed via SEM were dead. Extensive biofilm diffusion began after TTO@PCS treatment on day 1, with few poorly active viable bacteria remaining deep in the skin folds (Figure 5D and E). Although sampling of the skin surface covered with TTO@PCS on day 1 did not result in significant colonies on agar plates, colonies were observed again in day 3 samples. The bactericidal efficiency of TTO-NL@PCS was > 99%, suggesting that TTO-NL@PCS has rapid biofilm-dispersion abilities in the simulated biofilm model.

Internal Variation in Bacteria

To investigate the mechanism underlying the ability of TTO-NL@PCS to disrupt biofilms, ROS levels within the biofilm were monitored at different time points using DCFH-DA probes. A few green fluorescent spots were observed in the biofilm during the first 30 min of TTO-NL@PCS treatment, suggesting no obvious induction of ROS production

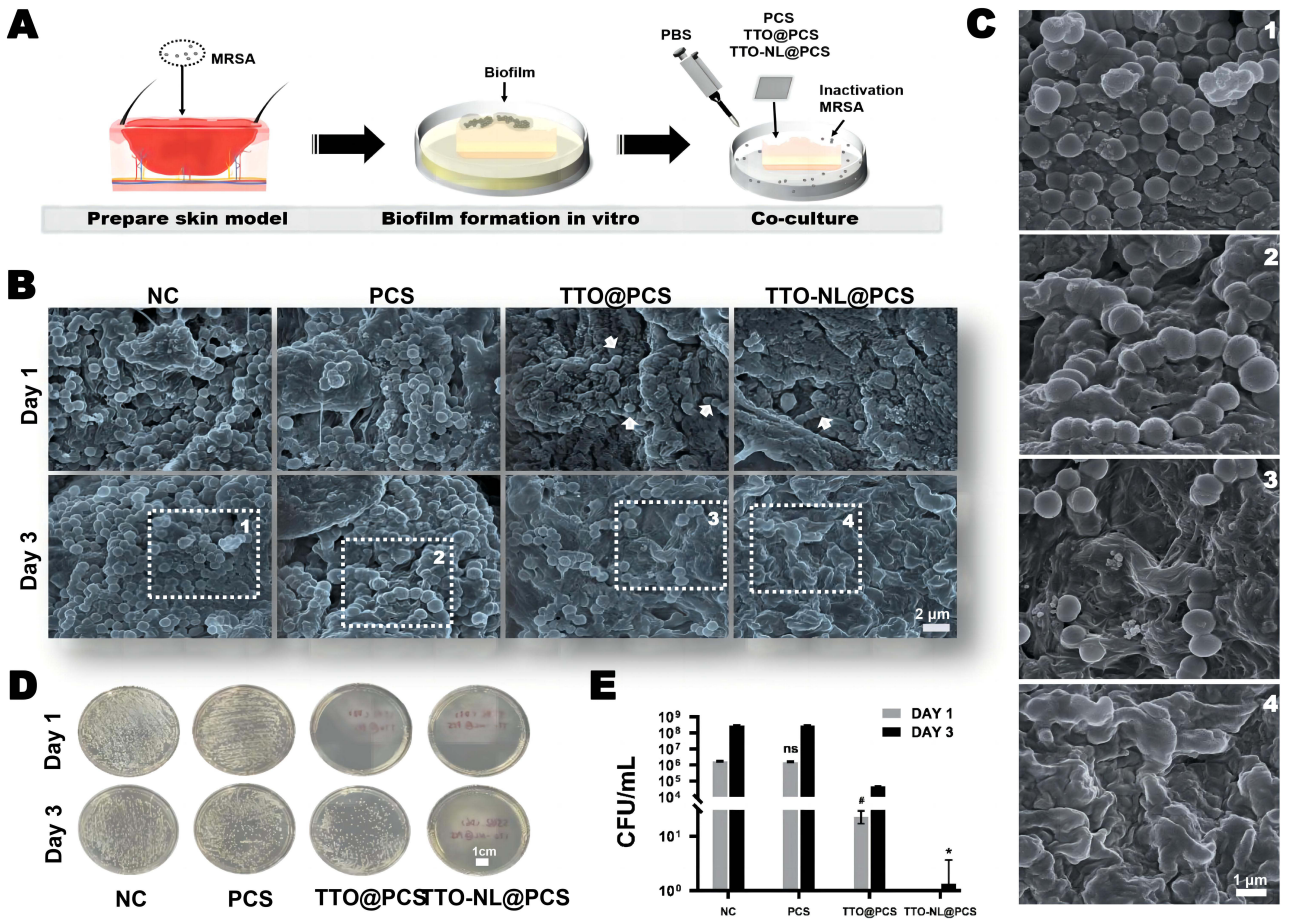

Figure 5 Assessment of the biofilm-dispersion activity of electrospun nanofibers in vivo. (**A**) Illustration of the biofilm-dispersion assay. (**B** and **C**) SEM observation of the remaining biofilm (ATCC 43300) on skin wounds when cultured with the electrospun sustained-release nanosystems at preset time points. White arrows indicate the bacteria remaining in the skinfolds. (**D** and **E**) Bacterial colonization in the skin tissues on days 1 and 3. n = 5, *P < 0.05 TTO-NL@PCS vs TTO@PCS, #P < 0.05 TTO@PCS vs NC, n.s. = no significance PCS vs NC.

(Figure 6A). Subsequently, ROS production increased exponentially, intensifying rapidly from 30 min (2.30 ± 0.23%) to 75 min (46.76 ± 0.30%; Figure 6B). Moreover, in the TTO-NL@PCS-treated biofilm, although ROS levels were low in the early stages, green fluorescence was detected in different biofilm layers, as observed in 3-D scans. At 30 min significant increases in ROS levels were observed in all layers (Figure 6C).

In vivo MRSA-Infected Diabetic Wound-Healing Study

We next explored the cytotoxic efficacy of TTO-NL@PCS against MRSA using BKS-Lepr ^{em2Cd479}/Gpt transgenic diabetic mice, which mimic a clinical wound model due to their efficient bactericidal ability in vitro (Figure 7A). No significant purulent exudates were observed in the TTO-NL@PCS- or TTO@PCS-treated wounds (Figure 7B). Owing to the self-healing capabilities of the wound-margin skin, all infected wounds had become markedly smaller by day 4 regardless of the treatment. Furthermore, TTO-NL@PCS-, TTO@PCS-, PCS-, and sham-treated wounds were almost completely healed at 16, 20, 23, and 26 days, respectively (Figure 7C). The body weights and blood glucose levels in the sham and PCS groups persistently decreased, and reduced activity was observed, which was possibly associated with concurrent sepsis; changes in body weights and blood glucose levels in TTO-NL@PCS- and TTO@PCS-treated mice were negligible (Figure 7D and E).

A pathological analysis of wound tissue through H&E staining reveal TTO-NL@PCS-treated wounds developed apparent skin islands and a nascent appendage structure on day 7, whereas the hair follicle structure was intact, and the epidermis was mostly healed on day 14. TTO@PCS-treated wounds healed relatively poorly with a relatively disordered

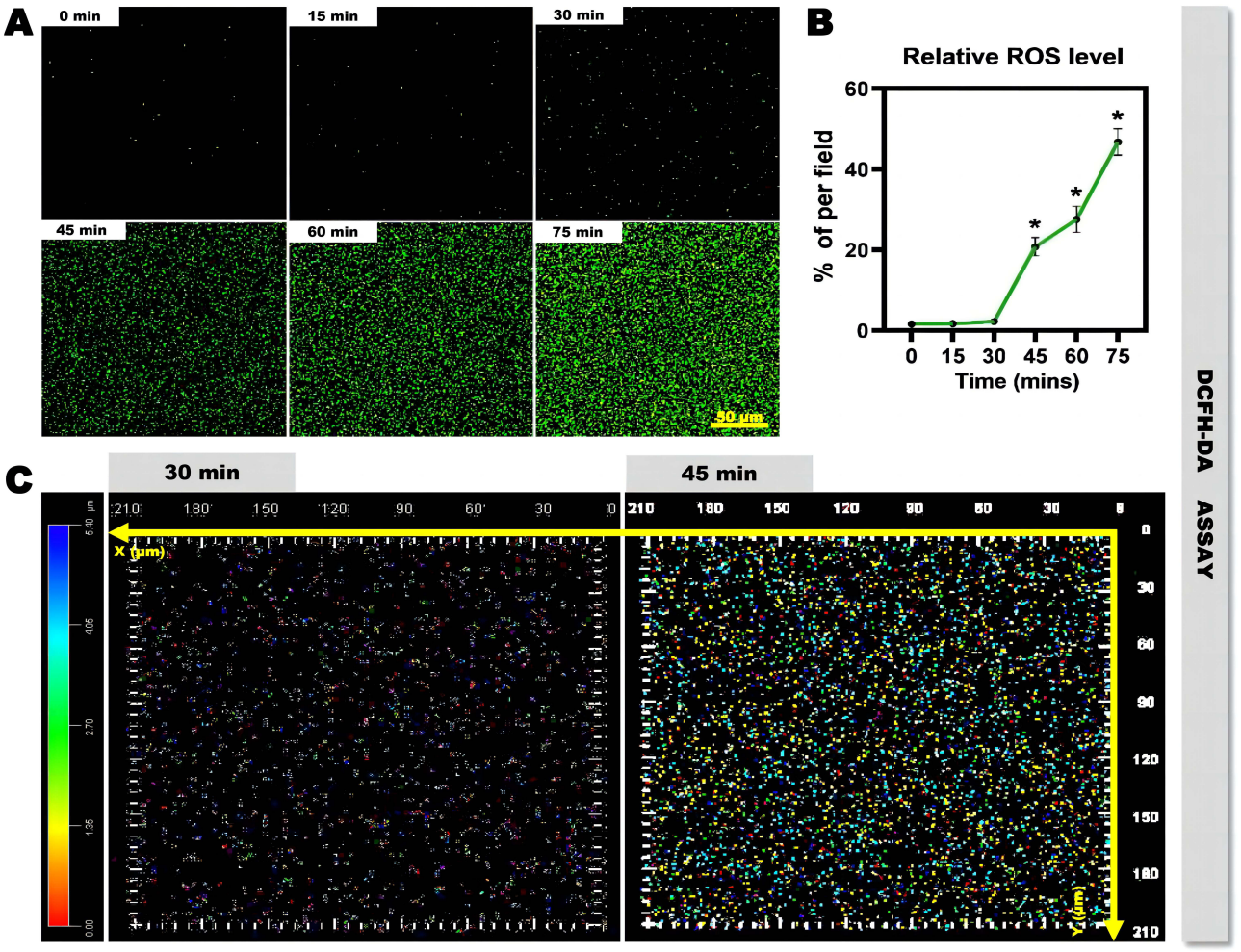

Figure 6 Investigation of the antibacterial mechanism. (**A**) Confocal images of ROS levels in the MRSA biofilm grown on cell slides after incubation with TTO-NL@PCS covered at preset time points. (**B**) The corresponding statistical fold chart showing relative ROS-level time variation. (**C**) ROS levels at different stages of biofilm formation, as obtained from 3-D scanning via LSCM. n = 3, *P < 0.05.

new skin structure (Figure 8A). More obvious necrotic tissues in the PCS and sham groups, and tissue-localized necrotic structures with massive macrophages and neutrophils were still observed on day 14 (Figure 8B). Immunofluorescence staining revealed early expression of VEGF in the TTO-NL@PCS-treated group with no significant differences among the other groups (Figure 8C and D).

Analysis of the Antibacterial Mechanism

To explore the relationship between the wound micrometabolic environment based on sterilization and healing, metabolomics analysis was conducted using 12 datasets from six biological replicates to determine the changes in metabolites present in the wound exudate after treatment with TTO-NL@PCS. The principal components analysis (PCA) results suggested high-quality data (Figure S2). In total, 87 differential metabolites were screened based on either FC 2.0 or FC 0.5, $P < 0.05$, and VIP values > 1.0 (Figure S3–6). Among the differentially expressed genes (DEGs; Figure S7), the expression of 26 metabolites was upregulated, while 61 were downregulated in the TTO-NL@PCS group relative to levels in the blank control group (Figure 9A). Among them, $PGF_{2\alpha}$ and 11-deoxy PGE_1 were the most significantly upregulated, with log_2FC values of 6.14 and 5.6, respectively (Figure 9B). Correlation analysis of the significantly different metabolites selected via Pearson correlation analysis was used to understand the synergistic or mutually exclusive relationship among these DEGs (Figure S8 and S9). Correlation analysis was beneficial for measuring the degree of metabolic closeness between significant and different metabolites, and metabolic proximities further helped to

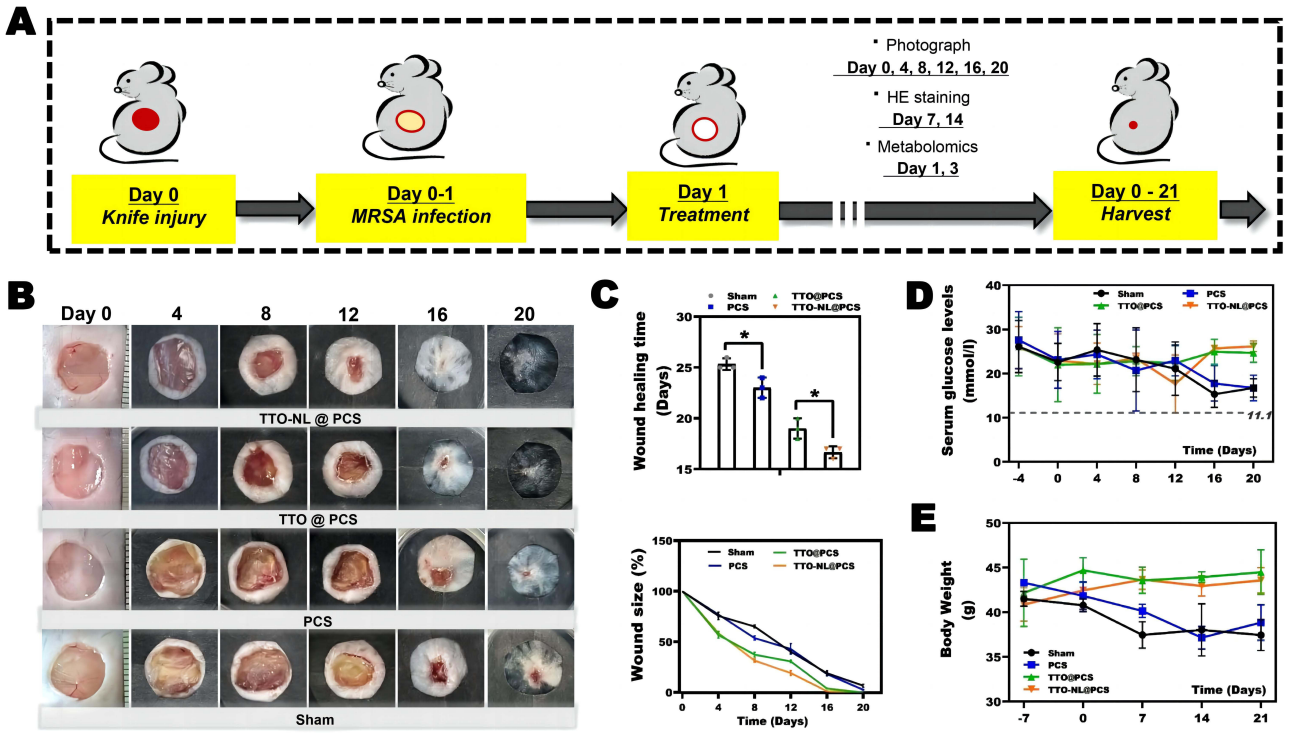

Figure 7 In vivo assessment of the bactericidal ability of electrospun nanofibers. (**A**) Schematic illustration of animal experiments. (**B**) Photographs of infected wounds, (**C**) wound-healing time, and corresponding statistical graphs of wound closure rates from the four groups subjected to different treatments after 0, 4, 8, 12, 16, and 20 days. Changes in (**D**) body weight and (**E**) serum glucose levels of the mice subjected to different treatments. n = 3, *P < 0.05.

elucidate the mutual regulatory relationship. Specifically, 19 enriched pathways, including steroid hormone biosynthesis ($P < 0.05$), were identified using KEGG enrichment analysis (Figure 9C).

Six hours after $PGF_{2\alpha}$ administration in the TTO-NL@PCS group, the mRNA expression levels of interleukin-1 (*IL-1*) and *IL-6* were significantly higher in wound tissues than in the sham group. Co-treatment with PGF2α and TTO-NL @PCS further increased the expression of *IL-1* and *IL-6* compared to those in mice administered TTO-NL@PCS or $PGF_{2\alpha}$ alone (Figure 10A–C). Moreover, immunofluorescence assays on the wound tissue sections indicated that PGF2α pretreatment improved the early local aggregation of neutrophils in the wound and facilitated targeted chemotaxis to the foci. The chemotactic aggregation of neutrophils was also observed early in the wound covered with TTO-NL@PCS; however, the local inflammatory response was promptly downregulated on day 7. The degree of early neutrophil aggregation was low, along with chemotaxis disorders, in the sham tissues (Figure 10D and E).

Discussion

Diabetic refractory ulcer co-infections necessitate an alternative technique to achieve the local release of antimicrobial drugs to disperse the mature biofilms and destroy bacteria deep in the wound from a therapeutic perspective.[44,45] Herein, TTO-NLs were successfully synthesized using ultrasonic shock and multiple high-pressure homogenization steps. Although TTO-NLs exhibit superior antibacterial and biofilm-dispersion activities, challenges including storage problems and volatility hinder their real-life applications.[46] Chitosan/polyvinyl alcohol nanofibers have attracted increasing attention due to their biodegradability, biocompatibility, antimicrobial activity, low immunogenicity, and wound-healing ability.[47] Electrospun TTO-NLs confer physical and biological advantages, achieving a balance among spinnability, function, and biological properties. Moreover, their high porosity-specific surface area facilitates convenient degradation with the assistance of collagenase in the wound and subsequent rupture to ensure the timely release of the drug. According to both AFM and SEM imaging results, the electrospun nanofibers had a structure similar to that of the fibrils in the native extracellular matrix (ECM), which also provided a large surface area to increase cell-material adhesion and interactions, as well as adjustable chemical, physical, and biological properties to regulate cellular activity,

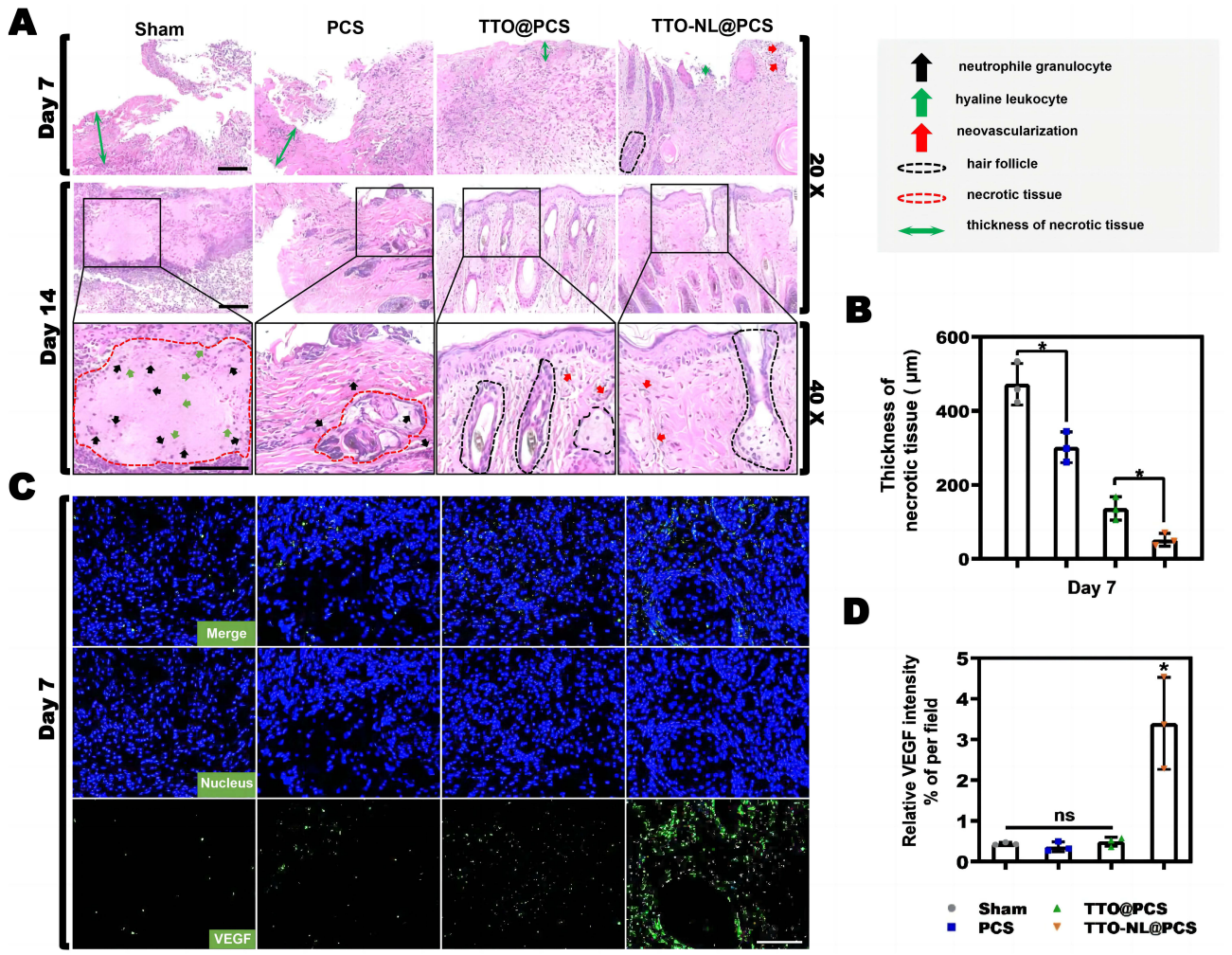

Figure 8 Histological and immunofluorescence analysis of wound skin. (**A**) H&E staining of the wound skin tissue on days 7 and 14 (scale bars, 50 μm). (**B**) Tissue thickness was quantified using ImageJ. n = 3, *P < 0.05. (**C**) Immunofluorescence images of wound tissues after treatment for 7 days (blue, nucleus; green, VEGF; scale bars, 100 μm) and (**D**) corresponding quantitative analysis of VEGF expression level. n = 3, *P < 0.05.
Abbreviation: n.s, no significance.

reshape ECM deposition, and promote tissue regeneration.[48] To mimic the topography[49] and function[50] of the ECM, a humid environment was provided, thus allowing gas exchange, avoiding bacterial infiltration, and manipulating immune-related processes in a pro-healing direction. Meanwhile, UV–Vis and GC analyses indicated slow release for 3 days without destruction of the drug constituents. TTO-NLs released from TTO-NL@PCS were subjected to secondary, short-acting sustained release to maintain the TTO concentration within the effective concentration range without eliciting cytotoxicity, while reaching deep wound layers to facilitate complete sterilization. Indeed, the encapsulation of TTO based on sustained release had no obvious detrimental effects on cell viability, proliferation, or chemotaxis. Accordingly, we propose that when multiple, slowly released TTO molecules spread systematically in the circulatory system, through the protective mechanism mentioned previously herein, higher TTO concentrations are applied to the focal area, thereby reducing cytotoxicity in a limited space.

The TTO-NL@PCS nano-platform has proven bactericidal, specifically against MRSA, through the extended release of TTO-NLs. More specifically, this treatment effectively kills > 80% of the bacteria within the first 6 h and 100% by 24 h. In comparison, the bactericidal efficacy of TTO@PCS was poor as it did not achieve a sufficient local concentration of TTO in the wound compared to that with TTO-NL@PCS. It can be argued that the loading of TTO into liposomes reduces loss during spinning. Bacteria within biofilms are less sensitive to antimicrobial agents than bacterioplankton due to drug osmotic restriction, drug extrusion, reduced oxygen and nutrient levels, reduced growth rates and metabolism,

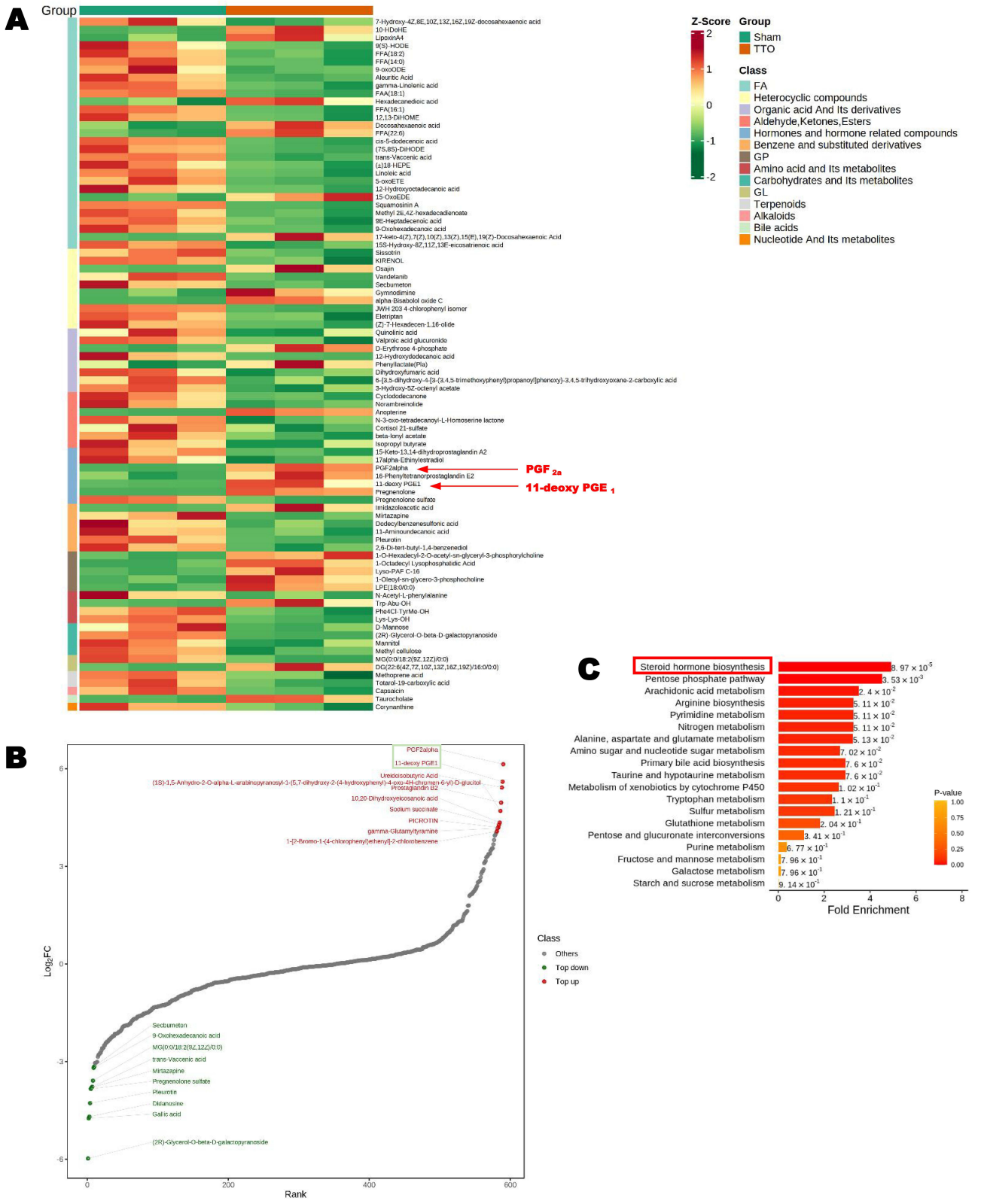

Figure 9 Metabolomics assay. Kyoto Encyclopedia of Genes and Genomes (KEGG, http://www.genome.jp/kegg/) was used for the pathway mapping of differential metabolites. Differential metabolites were labeled on the KEGG pathway map, with bright red indicating upregulation and bright green indicating downregulation. (2) Mapping of KEGG and PubChem (https://pubchem.ncbi.nlm.nih.gov/) metabolite databases with differential metabolites. Through the comprehensive analysis of pathways with differential metabolites (including enrichment analysis and topological analysis), pathways were further screened to identify key pathways with the highest correlation with differences in metabolites (**A**) Heatmap of the differential metabolite clusters. (**B**) Dynamic distribution map of the differences in metabolite contents. (**C**) MSEA plot.

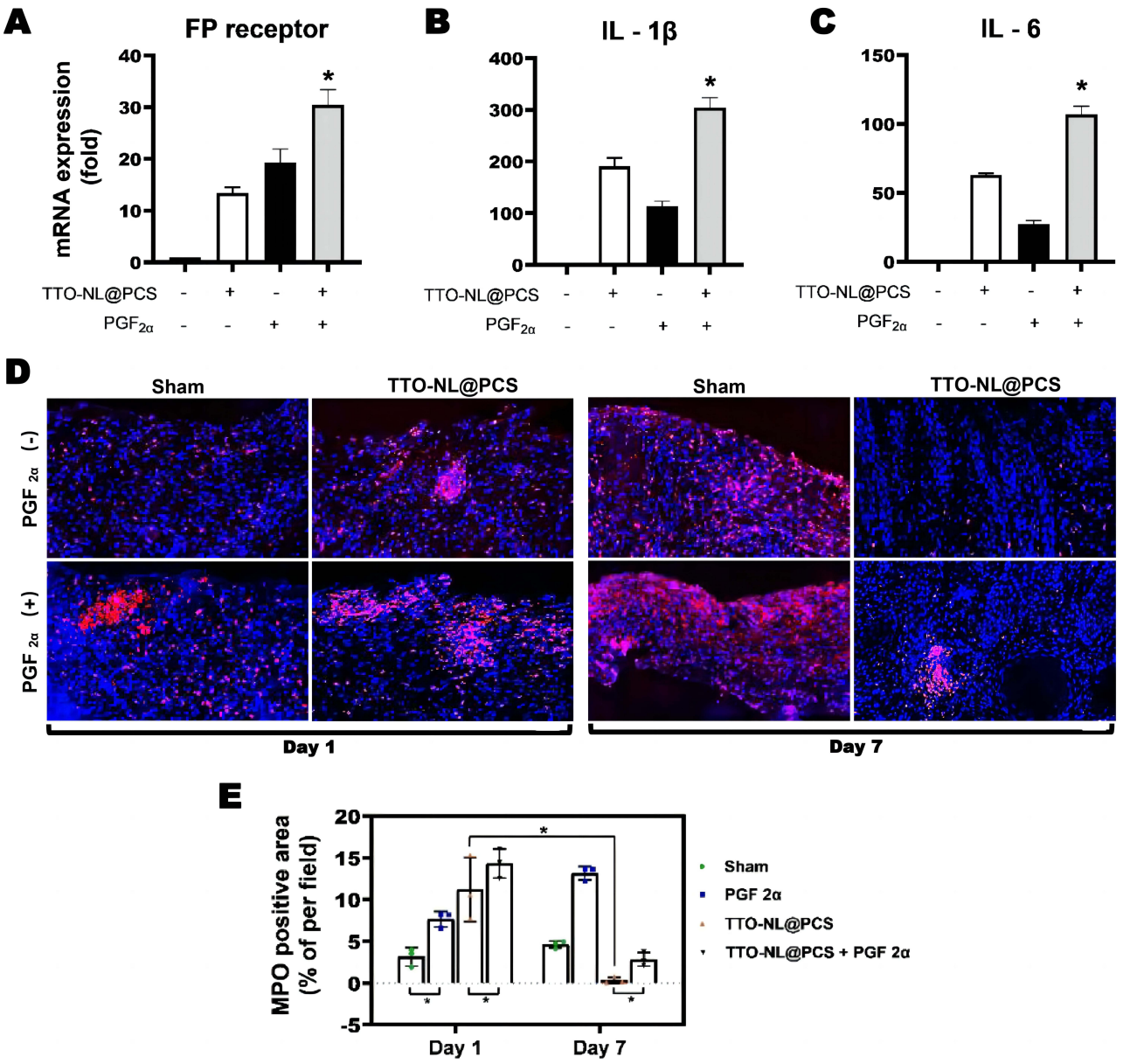

Figure 10 $PGF_{2\alpha}$-induced tissue inflammation. The mRNA level of FP receptor (**A**), IL-1β (**B**), and IL-6 (**C**) was measured via real-time PCR, 6 h after administration of $PGF_{2\alpha}$ (n = 3). *P < 0.05. (**D**) Representative pictures of immunofluorescence of the sections of wound skin on day 1 and 7 after administration of saline, $PGF_{2\alpha}$, and/or TTO-NL@PCS (scale bars, 50 μm). (**E**) Fluorescence for myeloperoxidase (MPO) was quantified at the indicated time points. n = 3, *P < 0.05.

quorum sensing, and the formation of persister cells.[51] Following in vitro biofilm simulations on skin wounds of patients with diabetes, SEM results revealed superior biofilm-dispersion and bactericidal effects, whereas in wounds sampled on the first day of TTO@PCS treatment, the lack of significant colony formation might have been associated with a self-dormancy mechanism. The former kills dormant bacteria in deep folds during the sustained release of drug components, suggesting that TTO-NL@PCS might exert significant antimicrobial effects when used in a clinical setting. After a short coverage time, the LSCM results through the 3-D layer sweep suggested that few bacteria survived in the MRSA biofilm. In the early stage of co-culture, TTO could penetrate deep biofilms. Elevated ROS levels in the biofilm or oxidative stress occurred in different layers after a period of treatment. Interestingly, the effect of TTO on elevated ROS levels in a short period was not obvious, which could be related to the physical resistance effect of the biofilm itself and to the drug efflux pumps. However, this resistance effect appears to have a cutoff value. Upon breakthrough, TTO quickly penetrates the internal body and widely acts on all dimensions, rapidly increasing the level of internal oxidative stress and causing

bacterial death. This rapid reduction in internal biofilm activity could help reduce the risk of drug resistance, especially when bacterial biofilms are thought to be the primary mechanism by which drug resistance occurs.[52]

To better evaluate the bactericidal and healing capacities in vivo, the TTO-NL@PCS composite nanoscale sustained-release system was applied as an antimicrobial dressing to model an acute MRSA infection of a full-thickness wound in diabetic mice. Healing was dynamically assessed by observing wounds, through H&E staining of the wound and pathological sections, and by exploring TTO-NL@PCS superiority via early-cell VEGF growth factor analysis. This model successfully showed the characteristics of the infection on days 7 and 14, including variability in the early degree of necrosis in the wound tissue and focal lacunar necrosis formation in the later stages. The wound imaging and healing time results showed that TTO-NL@PCS cleared the surface biofilm on day 7, promoted angiogenesis of the granulation tissue, and healed it by approximately day 16, which was markedly earlier than that observed in the sham group. In addition, on day 14, reasonably intact skin appendages developed, indicating that the natural structure of the skin regenerated better under the TTO-NL@PCS treatment regimen. This regimen also required less treatment time and exhibited antimicrobial efficacy, which could be due to the sustained-release mode maintaining a sufficient local antimicrobial concentration and the anti-inflammatory efficacy of TTO supporting the growth of new tissue. Moreover, the body weights and blood glucose levels in the treatment group remained stable, indicating that TTO might effectively restore the damage caused by bacterial exotoxin invasion of the wound and the reduced body weight.

Infected wound healing is a multicellular, growth factor-dependent, and extracellular matrix-dependent biological process.[53] The main cause of diabetic infection is a wound base regeneration disorder, specifically the inability to form efficient new granulation tissue. VEGF is a key factor in promoting neoangiogenesis for tissue regeneration, and the function of neovascularization in providing nutrition and oxygen is necessary for wound healing.[54,55] Histological analysis did not reveal significant complex residues in vivo, and the biodegradation behavior confirmed our in vitro results that TTO-NL@PCS was completely degraded within 7 days. In addition, drug-free PCS showed efficacy in inhibiting biofilm growth. Consistent with the results of previous correlation studies, the ability of cationic chitosan/polyvinyl alcohol electrospinning to chelate negatively charged metal ions can facilitate disruption of the cell wall and electrostatic interactions with the anionic lipopolysaccharide present in the outer membrane.[56] Additionally, electrostatic interactions between teichoic acids, one of the most important components of the peptidoglycan layer on the cell surface, lead to polyfactorial cell death.[57] Finally, at a certain weight, chitosan can penetrate the cell membranes of gram-negative bacteria, disrupting DNA/RNA synthesis and survival.[58] Taken together, the advantages of multi-mechanism bacterial killing and biofilm dispersion with a high level of biocompatibility suggest a potential for the TTO-NL@PCS composite nano-sustained-release system in clinical settings.

To further explore the mechanisms underlying wound sterilization and tissue healing, we collected exudates from wounds subjected to TTO-NL@PCS treatment for untargeted metabolomic analysis. Steroid hormone biosynthesis metabolism was enriched in the treatment group, along with the significant upregulation of $PGF_{2\alpha}$ synthesis; thus, it was speculated that TTO-NL@PCS achieved an autoimmune function with respect to neutrophil chemotaxis by enhancing local $PGF_{2\alpha}$ synthesis. Both the CCK-8 assay and enzyme-linked immunosorbent assay were used to determine the appropriate concentrations of exogenous $PGF_{2\alpha}$ to act on the wound surface, and $PGF_{2\alpha}$ was found to cooperate with TTO-NL@PCS. $PGF_{2\alpha}$ signaling is mediated by the $PGF_{2\alpha}$ receptor (PTGFR), which is coupled with the G protein Gq to activate various signaling pathways, including PLC/PKC, MAPKs, PI3K, and activated T-cell NFAT signaling.[59] FP receptors, a type of PTGFR, promote vascular senescence and induce cellular senescence, oxidative stress, and vascular remodeling through the upregulation of Src and PAI-1 expression. IL-1 induces the expression of many pro-inflammatory cytokines and chemokines, including IL-6, and upregulates COX-2 expression, leading to increased prostaglandin synthesis.[60,61] The results of this study indicated that in the initial stage of treatment, the TTO-NL@PCS composite nano-sustained-release system induces the rapid convergence of peripheral neutrophils to engulf the pathogen and necrotic tissue by upregulating the generation of chemokines IL-1 and IL-6, thereby alleviating the obstruction in neutrophil chemotaxis caused by the environmental imbalance in diabetes. Meanwhile, the rapid and thorough sterilization efficacy and anti-inflammatory efficacy of TTO help dissipate the neutrophils gathered in the wound in time and prevent chronic inflammation from hindering healing. However, the mechanism underlying the multi-

pathway interactions by which TTO exerts its effect within the body deserves further exploration to provide guidance for improving material synthesis.

Conclusion

In this study, we used high-voltage direct current electrospinning with polyvinyl alcohol/chitosan to successfully construct a composite nanoscale antibacterial sustained-release system with TTO-NLs; the broad-spectrum antibacterial activity, biofilm-dispersion ability, and healing-promoting capacity of the TTO-NLs were systematically verified. Using the BKS-Lepr^{em2Cd479}/Gpt mouse model of acute full-layer wounds combined with MRSA infection, we demonstrated that TTO-NL@PCS could kill bacteria deep in the skin folds, completely resolve the infection, and greatly reduce the healing time of refractory ulcers. This action could be attributed to disrupted biofilm integrity, the internal explosive production of ROS, and improved autoimmunity induced by the synthesis of $PGF_{2\alpha}$ in wounds. Moreover, TTO-NL@PCS has significant clinical therapeutic potential owing to its requirement for simple equipment and processes, efficient degradation, and minimal cytotoxicity. In conclusion, this study provides an effective antimicrobial treatment strategy that demonstrates remarkable advantages for the treatment of diabetic ulcers with MRSA infection.

Abbreviations

TTO, Tea tree oil; NLs, nanoliposomes; TTO-NLs, tea tree oil nanoliposomes; MRSA, methicillin-resistant *Staphylococcus aureus*; PBS, phosphate-buffered saline; trypsin-EDTA, trypsin-ethylenediaminetetraacetic acid; PCS, polyvinyl alcohol/chitosan spinning; GC, gas chromatography; FID, flame ionization detector; LSCM, laser scanning confocal microscopy; DAPI, 4′,6-diamidino-2-phenylindole; LB, lysogeny broth; CV, crystal violet; SEM, scanning electron microscopy; AFM, atomic force microscopy; 3D, three-dimensional; ATCC, American Type Culture Collection; CCK-8, Cell Counting Kit-8; CFU, colony forming unit; DLS, dynamic light scattering; H&E, hematoxylin and eosin; IL, interleukin; KCs, keratinocytes; ROS, reactive oxygen species; UV, ultraviolet; VEGF, vascular endothelial growth factor; ANOVA, analysis of variance; DFU, diabetic foot ulcer; ECM, extracellular matrix; EGFR, epidermal growth factor receptor; KEGG, Kyoto Encyclopedia of Genes and Genomes; TNF, tumor necrosis factor; MMP-1, matrix metalloproteinase 1; BSA, bovine serum albumin; MPO, myeloperoxidase; UPLC, ultra-performance liquid chromatography.

Data Sharing Statement

All additional information regarding data and materials is available upon request.

Funding

This work was supported, in whole or in part, by the Science and Technology Planning Project of Guangdong Province (Z.L; Grant Number 2017A020215042) and President Foundation of Nanfang Hospital, Southern Medical University (H. W; No: 2021C036).

Disclosure

The authors declare that they have no known competing financial interests or personal relationships that could have influenced the work reported in this study.

References

1. Liu Y, Zeng S, Ji W, et al. Emerging theranostic nanomaterials in diabetes and its complications. *Adv Sci*. 2022;9(3):e2102466. doi:10.1002/advs.202102466
2. Huang F, Lu X, Yang Y, et al. Microenvironment-based diabetic foot ulcer nanomedicine. *Adv Sci*. 2023;10(2):e2203308. doi:10.1002/advs.202203308
3. Berthiaume F, Hsia HC. Regenerative approaches for chronic wounds. *Annu Rev Biomed Eng*. 2022;24:61–83. doi:10.1146/annurev-bioeng-010220-113008
4. Trubenová B, Roizman D, Moter A, Rolff J, Regoes RR. Population genetics, biofilm recalcitrance, and antibiotic resistance evolution. *Trends Microbiol*. 2022;30(9):841–852. doi:10.1016/j.tim.2022.02.005
5. Bilyk B, Panchal V, Tinajero-Trejo M, Hobbs J, Foster SJM. An interplay of multiple positive and negative factors governs methicillin resistance in Staphylococcus aureus. *Microbiol Mol Biol Rev*. 2022;86(2):e0015921. doi:10.1128/mmbr.00159-21

6. Galar A, Weil A, Dudzinski D, Muñoz P, Siedner M. Methicillin-resistant staphylococcus aureus prosthetic valve endocarditis: pathophysiology, epidemiology, clinical presentation, diagnosis, and management. *Clin Microbiol Rev*. 2019;32(2):10–128. doi:10.1128/cmr.00041-18
7. Chen H, Yin Y, van Dorp L, et al. Drivers of methicillin-resistant Staphylococcus aureus (MRSA) lineage replacement in China. *Genome Med*. 2021;13(1):171. doi:10.1186/s13073-021-00992-x
8. Xiao J, Zhu Y, Huddleston S, et al. Copper metal-organic framework nanoparticles stabilized with folic acid improve wound healing in diabetes. *ACS Nano*. 2018;12(2):1023–1032. doi:10.1021/acsnano.7b01850
9. Roana J, Mandras N, Scalas D, Campagna P, Tullio V. Melaleuca alternifoliaAntifungal activity of essential oil (TTO) and its synergy with itraconazole or ketoconazole against. *Molecules*. 2021;26(2):461. doi:10.3390/molecules26020461
10. Carson C, Hammer K, Riley T. Melaleuca alternifolia (Tea Tree) oil: a review of antimicrobial and other medicinal properties. *Clin Microbiol Rev*. 2006;19(1):50–62. doi:10.1128/cmr.19.1.50-62.2006
11. Wilkinson J, Cavanagh H. Antibacterial activity of essential oils from Australian native plants. *Phytother Res*. 2005;19(7):643–646. doi:10.1002/ptr.1716
12. Lam N, Long X, Su X, Lu F. Biomedecine, pharmacotherapie, Melaleuca alternifolia (tea tree) oil and its monoterpene constituents in treating protozoan and helminthic infections. *Biomed Pharmacother*. 2020;130:110624. doi:10.1016/j.biopha.2020.110624
13. Vazquez J, Zawawi A. Efficacy of alcohol-based and alcohol-free melaleuca oral solution for the treatment of fluconazole-refractory oropharyngeal candidiasis in patients with AIDS. *HIV Clinic Trials*. 2002;3(5):379–385. doi:10.1310/99dy-8q52-306a-v0aj
14. Zhao L, Duan F, Gong M, et al. Bacillus cereus(+)-terpinen-4-ol inhibits biofilm formation by upregulating the interspecies quorum sensing signals diketopiperazines and diffusing signaling factors. *J Agric Food Chem*. 2021;69(11):3496–3510. doi:10.1021/acs.jafc.0c07826
15. Hylemon P. Harder, Biotransformation of monoterpenes, bile acids, and other isoprenoids in anaerobic ecosystems. *FEMS Microbiol Rev*. 1998;22(5):475–488. doi:10.1111/j.1574-6976.1998.tb00382.x
16. Yu D, Wang J, Shao X, Xu F, Wang H. Antifungal modes of action of tea tree oil and its two characteristic components against Botrytis cinerea. *J Appl Microbiol*. 2015;119(5):1253–1262. doi:10.1111/jam.12939
17. Hammer K, Carson C, Riley T. Effects of Melaleuca alternifolia (tea tree) essential oil and the major monoterpene component terpinen-4-ol on the development of single- and multistep antibiotic resistance and antimicrobial susceptibility. *Antimicrob Agents Chemother*. 2012;56(2):909–915. doi:10.1128/aac.05741-11
18. Pirker C, Hausen B, Uter W, et al. Sensibilisierung auf Teebaumol in Deutschland und Osterreich - Eine multizentrische Studie der Deutschen Kontaktallergiegruppe [Sensitization to tea tree oil in Germany and Austria. A multicenter study of the German Contact Dermatitis Group]. *J Dtsch Dermatol Ges*. 2003;1(8):629–634. doi:10.1046/j.1610-0387.2003.03727.x
19. de Groot A, Schmidt E. Tea tree oil: contact allergy and chemical composition. *Contact Derm*. 2016;75(3):129–143. doi:10.1111/cod.12591
20. Kalelkar P, Riddick M, García A. Biomaterial-based delivery of antimicrobial therapies for the treatment of bacterial infections. *Nat Rev Mater*. 2022;7(1):39–54. doi:10.1038/s41578-021-00362-4
21. Darvishi S, Tavakoli S, Kharaziha M, Girault H, Kaminski C, Mela I. Advances in the Sensing and Treatment of Wound Biofilms. 2022;61(13):e202112218. doi:10.1002/anie.202112218
22. Berini F, Orlandi V, Gornati R, Bernardini G, Marinelli F. Nanoantibiotics to fight multidrug resistant infections by Gram-positive bacteria: hope or reality? *Biotechnol Adv*. 2022;57:107948. doi:10.1016/j.biotechadv.2022.107948
23. Jia B, Du X, Wang W, et al. Nanophysical antimicrobial strategies: a rational deployment of nanomaterials and physical stimulations in combating bacterial infections. *Adv Sci*. 2022;9(10):e2105252. doi:10.1002/advs.202105252
24. Molinaro R, Evangelopoulos M, Hoffman J, et al. Design and development of biomimetic nanovesicles using a microfluidic approach. *Adv Mater*. 2018;30(15):e1702749. doi:10.1002/adma.201702749
25. Flores F, De Lima J, Da Silva C, et al. Hydrogels containing nanocapsules and nanoemulsions of tea tree oil provide antiedematogenic effect and improved skin wound healing. *J Nanosci Nanotechnol*. 2015;15(1):800–809. doi:10.1166/jnn.2015.9176
26. Elsabee M, Naguib H, Morsi R. Chitosan based nanofibers, review. *Mater Sci Eng C*. 2012;32(7):1711–1726. doi:10.1016/j.msec.2012.05.009
27. Greiner A, Wendorff J. Electrospinning: a fascinating method for the preparation of ultrathin fibers. *Angew Chem Int Ed*. 2007;46(30):5670–5703. doi:10.1002/anie.200604646
28. Geng X, Kwon O, Jang J. Electrospinning of chitosan dissolved in concentrated acetic acid solution. *Biomaterials*. 2005;26(27):5427–5432. doi:10.1016/j.biomaterials.2005.01.066
29. Kalantari K, Afifi A, Jahangirian H, Webster T. Biomedical applications of chitosan electrospun nanofibers as a green polymer. *Carbohydr Polym*. 2019;207:588–600. doi:10.1016/j.carbpol.2018.12.011
30. Jalvandi J, White M, Gao Y, Truong Y, Padhye R, Kyratzis I. Polyvinyl alcohol composite nanofibres containing conjugated levofloxacin-chitosan for controlled drug release. *Mater Sci Eng C Mater Biol Appl*. 2017;73:440–446. doi:10.1016/j.msec.2016.12.112
31. Jayakumar R, Prabaharan M, Sudheesh Kumar P, Nair S, Tamura H. Biomaterials based on chitin and chitosan in wound dressing applications. *Biotechnol Adv*. 2011;29(3):322–337. doi:10.1016/j.biotechadv.2011.01.005
32. Liu M, Sun C, Zheng X, et al. Macrobrachium rosenbergiiComparative proteomic analysis revealed the mechanism of tea tree oil targeting lipid metabolism and antioxidant system to protect hepatopancreatic health in Macrobrachium rosenbergii. *Front Immunol*. 2022;13:906435. doi:10.3389/fimmu.2022.906435
33. Davies N, Larkman T, Marriott P, Khan I. Determination of enantiomeric distribution of terpenes for quality assessment of Australian tea tree oil. *J Agric Food Chem*. 2016;64(23):4817–4819. doi:10.1021/acs.jafc.6b01803
34. Wong Y, West R, Chin S, Marriott P. Evaluation of fast enantioselective multidimensional gas chromatography methods for monoterpenic compounds: authenticity control of Australian tea tree oil. *J Chromatogr A*. 2015;1406:307–315. doi:10.1016/j.chroma.2015.06.036
35. Chen C, Han D, Cai C, Tang X. An overview of liposome lyophilization and its future potential. *J Control Release*. 2010;142(3):299–311. doi:10.1016/j.jconrel.2009.10.024
36. Wu J, Wang C, Chen K, et al. Electrospinning of quaternized chitosan-poly(vinyl alcohol) composite nanofiber membrane: processing optimization and antibacterial efficacy. *Membranes*. 2022;12(3):332. doi:10.3390/membranes12030332
37. Peesan M, Rujiravanit R, Supaphol P. Electrospinning of hexanoyl chitosan/polylactide blends. *J Biomater Sci Polym Ed*. 2006;17(5):547–565. doi:10.1163/156856206776986251

38. Bagchi B, Banerjee S, Kool A, et al. Synthesis of eucalyptus/tea tree oil absorbed biphasic calcium phosphate-PVDF polymer nanocomposite films: a surface active antimicrobial system for biomedical application. *Phys Chem Chem Phys*. 2016;18(25):16775–16785. doi:10.1039/c6cp03493d
39. Rodríguez-Maecker R, Vyhmeister E, Meisen S, Rosales Martinez A, Kuklya A, Telgheder UJA. Identification of terpenes and essential oils by means of static headspace gas chromatography-ion mobility spectrometry. *Anal Bioanal Chem*. 2017;409(28):6595–6603. doi:10.1007/s00216-017-0613-2
40. Grando T, Baldissera M, Gressler L, et al. Melaleuca alternifolia anthelmintic activity in gerbils experimentally infected by Haemonchus contortus. *Exp Parasitol*. 2016;170:177–183. doi:10.1016/j.exppara.2016.09.004
41. Jha S, Kanungo M, Nath A, D'Souza S. Entrapment of live microbial cells in electropolymerized polyaniline and their use as urea biosensor. *Biosens Bioelectron*. 2009;24(8):2637–2642. doi:10.1016/j.bios.2009.01.024
42. Souza M, Lopes L, Bonez P, et al. Melaleuca alternifolia nanoparticles against Candida species biofilms. *Microb Pathog*. 2017;104:125–132. doi:10.1016/j.micpath.2017.01.023
43. Oliva A, Costantini S, De Angelis M, et al. Melaleuca alternifoliaHigh potency of essential oil against multi-drug resistant gram-negative bacteria and methicillin-resistant. *Molecules*. 2018;23(10):2584. doi:10.3390/molecules23102584
44. Chen J, He J, Yang Y, et al. Antibacterial adhesive self-healing hydrogels to promote diabetic wound healing. *Acta Biomater*. 2022;146:119–130. doi:10.1016/j.actbio.2022.04.041
45. Maleki A, He J, Bochani S, Nosrati V, Shahbazi M, Guo B. Multifunctional photoactive hydrogels for wound healing acceleration. *ACS Nano*. 2021;15(12):18895–18930. doi:10.1021/acsnano.1c08334
46. Najafi-Taher R, Ghaemi B, Amani A. Delivery of Adapalene using a novel topical gel based on tea tree oil nano-emulsion: permeation, antibacterial and safety assessments. *Eur J Pharm Sci*. 2018;120:142–151. doi:10.1016/j.ejps.2018.04.029
47. Campa-Siqueiros P, Madera-Santana T, Castillo-Ortega M, López-Cervantes J, Ayala-Zavala J, Ortiz-Vazquez E. Electrospun and co-electrospun biopolymer nanofibers for skin wounds on diabetic patients: an overview. *RSC Adv*. 2021;11(25):15340–15350. doi:10.1039/d1ra02986j
48. Nagarajan S, Belaid H, Pochat-Bohatier C, et al. Design of boron nitride/gelatin electrospun nanofibers for bone tissue engineering. *ACS Appl Mater Interfaces*. 2017;9(39):33695–33706. doi:10.1021/acsami.7b13199
49. Friedl P, Wolf K. Plasticity of cell migration: a multiscale tuning model. *J Cell Biol*. 2010;188(1):11–19. doi:10.1083/jcb.200909003
50. Scadden DT. Nice neighborhood: emerging concepts of the stem cell niche. *Cell*. 2014;157(1):41–50. doi:10.1016/j.cell.2014.02.013
51. Li X, Chen D, Xie S. Current progress and prospects of organic nanoparticles against bacterial biofilm. *Adv Colloid Interface Sci*. 2021;294:102475. doi:10.1016/j.cis.2021.102475
52. Blackman L, Qu Y, Cass P, Locock K. Approaches for the inhibition and elimination of microbial biofilms using macromolecular agents. *Chem Soc Rev*. 2021;50(3):1587–1616. doi:10.1039/d0cs00986e
53. Zhao R, Kong W, Sun M, et al. Highly stable graphene-based nanocomposite (GO-PEI-Ag) with broad-spectrum, long-term antimicrobial activity and antibiofilm effects. *ACS Appl Mater Interfaces*. 2018;10(21):17617–17629. doi:10.1021/acsami.8b03185
54. Wang C, Wang M, Xu T, et al. Engineering bioactive self-healing antibacterial exosomes hydrogel for promoting chronic diabetic wound healing and complete skin regeneration. *Theranostics*. 2019;9(1):65–76. doi:10.7150/thno.29766
55. Gurtner G, Werner S, Barrandon Y, Longaker MJN. Wound repair and regeneration. *Nature*. 2008;453(7193):314–321. doi:10.1038/nature07039
56. Liu H, Du Y, Wang X, Sun L. Chitosan kills bacteria through cell membrane damage. *Int J Food Microbiol*. 2004;95(2):147–155. doi:10.1016/j.ijfoodmicro.2004.01.022
57. Raafat D, von Bargen K, Haas A, Sahl H. Insights into the mode of action of chitosan as an antibacterial compound. *Appl Environ Microbiol*. 2008;74(12):3764–3773. doi:10.1128/AEM.00453-08
58. Verlee A, Mincke S, Stevens C. Recent developments in antibacterial and antifungal chitosan and its derivatives. *Carbohydr Polym*. 2017;164:268–283. doi:10.1016/j.carbpol.2017.02.001
59. Flower L, Gray R, Pinkney J, Mohamed-Ali VJC. Stimulation of interleukin-6 release by interleukin-1beta from isolated human adipocytes. *Cytokine*. 2003;21(1):32–37.
60. Kniss D, Zimmerman P, Garver C, Fertel R. Interleukin-1 receptor antagonist blocks interleukin-1-induced expression of cyclooxygenase-2 in endometrium. *Am J Obstet Gynecol*. 1997;177(3):559–567. doi:10.1016/s0002-9378(97)70146-7
61. Molnár M, Romero R, Hertelendy F. Interleukin-1 and tumor necrosis factor stimulate arachidonic acid release and phospholipid metabolism in human myometrial cells. *Am J Obstet Gynecol*. 1993;169(4):825–829. doi:10.1016/0002-9378(93)90011-7

International Journal of Nanomedicine Dovepress

Publish your work in this journal

The International Journal of Nanomedicine is an international, peer-reviewed journal focusing on the application of nanotechnology in diagnostics, therapeutics, and drug delivery systems throughout the biomedical field. This journal is indexed on PubMed Central, MedLine, CAS, SciSearch®, Current Contents®/Clinical Medicine, Journal Citation Reports/Science Edition, EMBase, Scopus and the Elsevier Bibliographic databases. The manuscript management system is completely online and includes a very quick and fair peer-review system, which is all easy to use. Visit http://www.dovepress.com/testimonials.php to read real quotes from published authors.

Submit your manuscript here: https://www.dovepress.com/international-journal-of-nanomedicine-journal